



Aalto University
School of Electrical
Engineering

AALTO UNIVERSITY

School of Electrical Engineering

Department of Radio Science and Engineering

Mohammad Arif Saber

Thermal characterization of THz planar Schottky diodes using simulations

Master's Thesis

Espoo, 30.11.2012

Supervisor: Professor Antti Räisänen, Aalto University, Finland

Instructor : D.Sc. (Tech) Juha Mallat, Aalto University, Finland



AALTO UNIVERSITY
School of Electrical Engineering
Department of Radio Science and Engineering

ABSTRACT OF
MASTER'S THESIS

Author: Mohammad Arif Saber

Title of Thesis:

Thermal characterization of THz planar Schottky diodes using simulations.

Date: 30.11.2012

Pages: 60

Professorship: Radio Engineering

Code: S-26

Supervisor: Professor Antti Räisänen

Instructor: D.Sc. (Tech) Juha Mallat

Schottky diodes are preferred and used in heterodyne receivers as a mixing element. In higher frequencies (THz band) the size of the diode especially the anode junction, becomes very small and causes reduced thermal properties compared to its lower frequency counterparts. Self heating for these high frequency diodes becomes very significant for even a very small amount of current.

In this master's thesis different methods of thermal and electrical characterization have been studied. Also different thermal characteristics like junction temperature, thermal resistance and thermal time constant have been investigated through simulations. COMSOL is the elected software for the simulations.

Two commercial diodes have been analyzed and different methods of simulating the thermal properties have been discussed and presented. Also some comparisons with measurement results have been carried out. However, in all these thermal simulations the diode current is kept constant and only DC simulations have been carried out.

Keywords: Schottky diode, thermal characterization, thermal resistance, thermal time constant, self heating, junction temperature

Language: English

Acknowledgements

This master's thesis has been carried out in the Department of Radio Science and Engineering of Aalto University School of Electrical Engineering. This thesis is linked to a MilliLab project which has been done in close co-operation with the European Space Agency (ESA) and Technical Research Center of Finland (VTT).

First of all, I would like to express my sincere gratitude to my supervisor, Prof. Antti Räsänen, for giving me the opportunity to work under his supervision. Also I would thank him for his guidance and wisdom.

I would also like to thank my instructor D.Sc.(Tech) Juha Mallat for his guidance, encouragements, ideas and advice. Also I would like to thank him for keeping patient with me during the research process. Furthermore my cordial thanks and gratitude goes to D.Sc.(Tech). Tero Kiuru, Ms. Krista Dahlberg and Mr. Subash Khanal for their help, support and contribution during the work.

Also special thanks are due to my parents for their continuous support, encouragement and blessing to get me through with not only the thesis but also my life. I also thank my friends for always being there for me.

Finally, I would also like to thank all the members of the Bangladeshi community at Aalto University for their valuable suggestions, support and encouragement.

Otaniemi, Espoo; 19.11.2012

Mohammad Arif Saber

Contents

Abstract	2
List of Tables	6
List of Figures	7
Abbreviations and Acronyms	10
1 Introduction	12
1.1 Motivation and scope	12
1.2 Structure of the thesis	13
2 Terahertz planar Schottky diodes	14
2.1 Overview of planar Schottky diode operation	14
2.1.1 Metal semiconductor contact	14
2.1.2 Current voltage characteristics	16
2.1.3 Series resistance	17
2.2 Thermal properties of THz planar Schottky diode	18
2.3 Different methods for thermal characterization	19
2.3.1 Full wave modeling	20
2.3.2 Physical contact method	20
2.3.3 Electrical junction temperature measurement	21
2.3.4 Liquid crystal imaging method	21
2.3.5 Method based on S-parameter and temperature controlled measurements	22
2.3.6 Pulsed I-V measurements	22
2.4 Analysis for different thermal properties	22

2.4.1	Steady state thermal analysis	22
2.4.2	Transient thermal analysis	23
3	Modeling and analysis methodology	25
3.1	Modeling of a simple diode	25
3.2	Modeling with only heat transfer	27
3.3	Modeling with heat transfer and electric currents	28
3.4	Modeling with COMSOL Multiphysics	28
4	Results and discussions	32
4.1	Temperature distribution on diode surface	32
4.2	Simulations related to thermal resistance	40
4.3	Variation of the epilayer	42
4.4	Variation in anode finger	44
4.5	Temperature rise as a function of time	46
4.6	Thermal time constant extraction	48
4.7	Different heating time	50
4.8	Comparison with the measured results	52
5	Conclusion and future work	56
	Bibliography	58

List of Tables

3.1	Structural parameters of different layers of test diode A	26
3.2	Material properties of different layers of diode model test diode A	27
4.1	Structural parameters of a simple structure to find out the heat loss	34
4.2	Effects of degrees of freedom to be solved in simulation time for voltage of 1 V and current of 5 mA	36
4.3	Effects of degrees of freedom to be solved in simulation time for voltage of 1 V and current of 1 mA	37
4.4	Material properties of different layers of diode model test diode C	37
4.5	Material properties of different layers of diode model test diode B	40
4.6	Simulation time (time dependent simulations) of Test diode C with different number of degrees of freedom and varying step size	47
4.7	Extracted thermal time constants	49
4.8	Extracted thermal time constants for measured results	54

List of Figures

2.1	Energy band diagram of metal-semiconductor (n-type) contact. In a) metal and semiconductor are not in contact, in b) metal and semiconductor are connected and form a single system [1].	15
2.2	Energy band diagram of metal-semiconductor (n-type) contact. In a) metal-semiconductor junction is reverse biased, and in b) metal-semiconductor junction is forward biased [1].	16
3.1	Test diode A containing all the basic layers (anode, cathode, insulation, buffer, epi layer) (left); wire frame view of the diode (right).	26
3.2	Modeling with COMSOL. 1st: import geometry, 2nd: adding material, 3rd: adding material to different layer of the model, 4th: defining mesh for different layers of the model, 5th: adding physics, 6th: defining physics in the model, 7th: adding solvers.	29
3.3	Flowchart representing process for COMSOL modeling.	30
3.4	Assumed diode parameters for test diode A.	31
3.5	Process to find out junction temperature(left). Incorporating current-voltage relationship in COMSOL (right).	31
4.1	Temperature distribution on the surface of test diode A (current 5 mA and voltage 1 V).	32
4.2	Cross section of the simple diode split in XZ plane with different lines of measurement of temperature.	33
4.3	Temperature distribution along different lines described in Figure 4.2 for 5 mW input power.	33
4.4	Slice of the diode for temperature distribution in XZ plane with 5 mW input power.	34
4.5	Simple structure model to find out the temperature loss. (a) Side view of the simple structure, (b) top view of the structure and (c) back view of the structure.	35

4.6	Variation of junction temperature with buffer layer radius for the simple structure with 1 V and 10 mA.	35
4.7	Variation of junction temperature with anode height for the simple structure with 1 V and 10 mA.	36
4.8	Cross section of test diode C split into half in XZ plane with lines of measurement of temperature.	38
4.9	Temperature distribution of test diode C along the line described in Figure 4.8.	38
4.10	Metal housing structure with dimensions.	39
4.11	Metal housing structure with dimensions.	39
4.12	Structure of test diode B. A: Side view of the diode under quartz. B: Side view of the diode. C: Top view of the diode mounted on quartz. D: Top view of the diode.	40
4.13	Junction temperature with variation of power for test diode B.	41
4.14	Thermal resistance with the variation of power for test diode B.	41
4.15	Junction temperature with variation of power for test diode C.	42
4.16	Thermal resistance with the variation of power for test diode C.	42
4.17	Diode current with time while using 1 V and epilayer resistance changed to get 10 mA current.	43
4.18	Test diode A temperature vs time with the variation of epilayer height with voltage 1 V, current 10 mA, and 1 μ s pulse length.	43
4.19	Test diode B temperature vs time with the variation of epilayer height with voltage 1 V, current 10 mA, and 1 μ s pulse length.	44
4.20	Test diode A temperature vs time with the variation of epilayer radius with voltage 1 V, current 10 mA, and 1 μ s pulse length.	44
4.21	Test diode A temperature vs time with the variation of anode finger length with voltage 1 V, current 10 mA, and 1 μ s pulse length.	45
4.22	Test diode A temperature vs time with the variation of anode finger width with voltage 1 V, current 10 mA, and 1 μ s pulse length.	45
4.23	Temperature as a function of time for test diode B.	46
4.24	Test diode B temperature rise with time.	47
4.25	Test diode C temperature rise with time.	48
4.26	Test diode C thermal time constant extraction with MATLAB curve fitting for simulated results.	49
4.27	Test diode B junction temperature fall for different heating time.	50

4.28	Test diode B temperature fall time in log scale.	50
4.29	Test diode B peak junction temperature after different heating time.	51
4.30	Test diode C cooling curves for different heating time.	51
4.31	Test diode C temperature response from cooling curves.	52
4.32	Comparison of measured and simulated results with 6.74 mW of power of test diode C temperature rise with time.	53
4.33	Comparison of measured and simulated results with 6.74 mW of power of test diode C thermal resistance.	54
4.34	Test diode C thermal time constant with MATLAB curve fitting for measured results.	55

Abbreviations and list of symbols

Abbreviations

AlGaAs	Aluminium Gallium Arsenide
CPW	Coplanar waveguide
DC	Direct current
ESA	European Space Agency
GaAs	Gallium Arsenide
MilliLab	Millimetre Wave Laboratory of Finland
RF	Radio frequency
SiO ₂	Silicon dioxide
THz	Terahertz
TSP	Temperature sensitive parameter

List of symbols

A^{**}	Effective Richardson constant
$C_p(T)$	Thermal capacity
I_d	Diode current
I_s	Saturation current
k_B	Boltzmann's constant
N_d	Doping concentration
P_T	Dissipated power
q	Elementary charge
r_a	Anode radius
R_s	Series resistance
R_θ	Thermal resistance
T_0	Ambient temperature
T_j	Junction temperature
V_j	Junction voltage
η	Ideality factor
ρ_θ	Thermal resistivity
τ	Thermal time constant
ϕ_B	Barrier height
ϕ_{bi}	Built-in voltage
ϕ_m	Metal work function
ϕ_s	Semiconductor work function
χ	Electron affinity

Chapter 1

Introduction

In physics, terahertz radiation refers to the propagation of electromagnetic waves frequencies in the terahertz range, from 0.3 to 3 THz. In wavelengths, the range spans from 0.1 mm (or 100 μm) to 1.0 mm. Potential THz applications can be medical imaging, security scanning, radio astronomy, earth science applications and ultra-fast communications [2, 3, 4]. Millimeter waves have several advantages over their longer wavelength counterparts. It results in miniaturizing key components like antennas as well as higher data rate in communications [5].

As Schottky diode technology moves towards higher frequencies the anode junction area of the diode is reduced. The smaller anode size has an adverse effect on its thermal capabilities. The reduced thermal performance and subsequent self heating of the diode imposes some challenges. The traditional I-V and C-V measurements do not provide with reliable results and thermal constraints limits the attainability of the electrical performance. That is why new methods should be developed to characterize and accurately estimate the diode parameters and junction temperature with known input power levels. Optimization of performance of the THz planar Schottky diodes as well as frequency dependent losses and current crowding effect are discussed in [6].

This thesis work is devoted to develop a better understanding of the THz planar Schottky diode's thermal characteristics using simulations. At the end the simulated results are compared with measurement results to accredit the research work.

1.1 Motivation and scope

In this thesis the prevailing methods like physical modeling, electrical measurements and imaging methods are reviewed. The advantages and disadvantages of these methods are analyzed. The suitability of characterization of THz varactor and mixer Schottky diodes are evaluated.

Thermal simulations are a valuable tool for evaluating the thermal performance of different

Schottky diodes and for increasing the understanding of heat flow paths. This information will provide data, against which the measurement results can be compared. Two commercial diodes, a varactor and a mixer diode, have been simulated. Only DC simulations are carried out throughout this thesis as the key thermal parameters such as junction temperature, thermal impedance and thermal time constant are to be found out. This work does not look into current crowding effect and frequency dependent losses. That is beyond the scope of this thesis. Furthermore, this thesis does not cover the optimization of the diode structure and properties. Also variation for different thermal properties for these diodes are also not studied in this thesis. This thesis is related to the project work MilliLab framework work order 3 "Thermal and electrical characterization for Schottky diodes".

1.2 Structure of the thesis

The thesis presents thermal modeling of a THz planar Schottky diode. Three thermal parameters are of key importance in this thesis. The thermal parameters are thermal impedance, junction temperature and thermal time constants.

In Chapter 1 background, motivation and scope of this thesis are described, and applications of THz Schottky diodes and related challenges are presented.

Chapter 2 provides a general description of thermionic emission theory, current voltage (I-V) characteristics of the Schottky diode, basic Schottky diode operation principle and series resistance of Schottky diode. Different thermal characterization methods applied previously are also described. Analysis for different thermal properties like thermal time constant and junction temperature determination has been also presented in this chapter.

Chapter 3 is concerned with models and analysis methodology used in this work. Different processes to tackle the problem are presented in this chapter along with description on how modeling is done in COMSOL Multiphysics.

Chapter 4 presents the corresponding results and analysis that is performed in this research work. Thermal analysis has been done for two commercial diodes a mixer and a varactor. Here also a simple diode structure is built and analyzed for different thermal properties. First some simulations are done to validate the work. Then simulations are done for different conditions and for different thermal properties. Lastly, comparison between some measurement results have been introduced and a level of uncertainty with the measured results is tried to find out. Chapter 5 concludes the research work and discusses future work.

Chapter 2

Terahertz planar Schottky diodes

In 1904, the first practical semiconductor device was introduced and it was a metal-semiconductor contact which showed a certain rectifying behavior. The device was a metallic whisker pressed against a semiconductor which became very popular for the applications. In 1938, Schottky suggested that the rectifying behavior could arise from a potential barrier [1]. This was later named as Schottky diode. In this chapter the operation of Schottky diode and different thermal characterization methods are discussed.

2.1 Overview of planar Schottky diode operation

The Schottky diode operation is a result of charge transport mechanism of metal-semiconductor contact which is also known as Schottky barrier. Schottky diodes can be divided into resistive (varistor) and varactor diodes. A varactor is a variable capacitor device in which the frequency conversion is based on capacitance modulation. The resistive diodes are also known as mixer diodes. In this thesis two commercial diodes, a mixer and a varactor diode have been analyzed along with a simple built diode structure to validate different results.

2.1.1 Metal semiconductor contact

The contact between the metal and semiconductor results into a potential barrier. This potential barrier is responsible for the Schottky diode current voltage (I-V) and capacitance-voltage (C-V) characteristics. In this section the operation under bias voltage and barrier formation is discussed shortly. The physics behind Schottky diode operation is in detail discussed in [7, 8, 9].

When the metal and the n-type doped semiconductor are separated from each other the metal semiconductor band diagram looks very different from the band diagram when they are in contact with each other. See Figure 2.1. This band diagram is in detail discussed in [10].

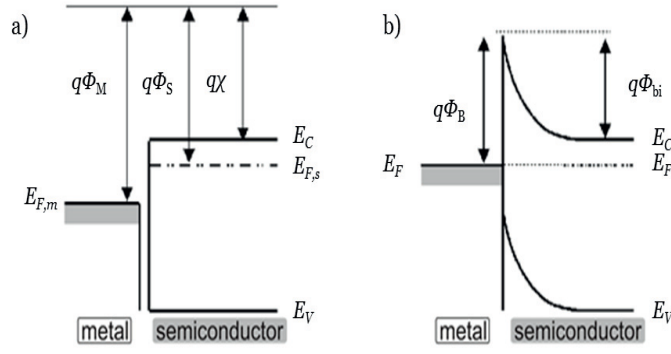


Figure 2.1: Energy band diagram of metal-semiconductor (n-type) contact. In a) metal and semiconductor are not in contact, in b) metal and semiconductor are connected and form a single system [1].

Metal work function $q\phi_m$ is not in the same level with the n-type semiconductor work function $q\phi_s$. The work function is the energy difference between the Fermi level and vacuum level. Also the electron affinity $q\chi_s$ which is the energy difference between the electron conduction band edge and the vacuum level of the semiconductor is shown in Figure 2.1 [1].

When the metal and semiconductor make intimate contact, the Fermi level of the metal and semiconductor must be equal at thermal equilibrium. Also the vacuum level should be continuous. These two requirements determine a unique energy band diagram of the ideal metal-semiconductor contact [1]. Also when the Fermi level of the semiconductor is lowered to the same level as the Fermi level in the metal, the flow of electrons stops. The electrons on the metal of the contact create a potential barrier for the electrons in the semiconductor. This barrier is called the built-in voltage. The built-in voltage can be calculated by equation (2.1).

$$q\phi_{bi} = q\phi_m - q\phi_s. \quad (2.1)$$

The electrons in the metal also suffer a potential barrier with the height of

$$q\phi_B = q(\phi_m - \chi), \quad (2.2)$$

where q is the elementary charge and χ is the electron affinity. The barrier height is also known as the Schottky barrier. The flow of electrons from semiconductor to metal causes part of the semiconductor to gain positive net charge. The positively charged region which is created by this flow of electrons is also known as the depletion region. The width of the depletion region plays a very important role in the function of a Schottky diode.

The Schottky diode can be biased in two different ways. When the diode is forward biased and voltage V_b is applied the energy is increased by qV_b . Electrons with less energy are less likely to move across the potential barrier than electrons with more energy and vice versa. This increases the current through the junction as the voltage is increased. Under different bias voltage the

depletion region width can be calculated as

$$w_d = \sqrt{\frac{2\epsilon_s(\phi_{bi} - V_b - k_B T_j / q)}{qN_D}}, \quad (2.3)$$

where ϵ_s is the permittivity of the semiconductor, k_B is Boltzmann's constant, T_j is the temperature of the junction and N_D is the donor doping density.

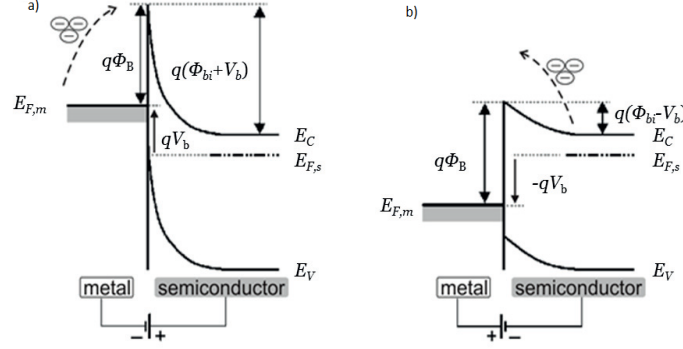


Figure 2.2: Energy band diagram of metal-semiconductor (n-type) contact. In a) metal-semiconductor junction is reverse biased, and in b) metal-semiconductor junction is forward biased [1].

The energy band diagram of metal-semiconductor (n-type) in forward and reversed bias looks like Figure 2.2 which is further described in [10] and not discussed in this thesis any further.

2.1.2 Current voltage characteristics

Under a forward bias, thermionic emissions, recombination in the space charge region and recombination in the neutral region occurs in the current transport mechanism [11]. For a good metal-semiconductor contact, the overall transport mechanism is believed to be dominated by the thermionic emissions. Thermionic emission model of the Schottky diode is described in [7, 12]. The current voltage (I-V) equation can be simply written as

$$I_d(V_j, T) = I_s \left(e^{\frac{qV_j}{\eta k_B T}} - 1 \right) \quad (2.4)$$

$$I_s(T) = AA^{**} T^2 e^{-\frac{q\phi_B}{k_B T}}, \quad (2.5)$$

where I_d is the total diode current, I_s is the saturation current, V_j is junction voltage, η is the ideality factor of the diode, A is the junction area, A^{**} is the effective Richardson constant ($8.2 \text{ Acm}^{-2}\text{K}^{-2}$ for GaAs), T is the absolute temperature, ϕ_B is the barrier height and k_B is Boltzmann's constant.

In case of a thermionic emission dominating the electrontransport mechanism, the ideality factor is close to unity. But this is not the case in practical scenario. The effect of doping and concentration and temperature in a ideality factor is formulated in [13] as:

$$\eta = \frac{1}{(k_B T) \left(\frac{\tanh\left(\frac{E_{00}}{k_B T}\right)}{E_{00}} - \frac{1}{2E_B} \right)} \quad (2.6)$$

$$E_{00} = 18.5 \times 10^{-12} \sqrt{\frac{N_d}{m_e^* \epsilon_r}}, \quad (2.7)$$

where E_{00} is a material constant with constant doping density, E_B is band bending, m_e^* is the electron effective mass, and ϵ_r is semiconductor relative permittivity.

The bias current is responsible for the self heating in effect. The saturation current and the ideality factor plays a very important role in defining the bias current.

2.1.3 Series resistance

The diode series resistance contains several key elements, each play a different and significant role. There are three components which build the series resistance which can be expressed by the following equation

$$R_s(V_j, f) = R_{spreading}(f) + R_{contact}(f) + R_{epi}(V_j, f), \quad (2.8)$$

where R_{epi} is the junction epitaxial-layer resistance, $R_{spreading}$ is the buffer layer spreading resistance and $R_{contact}$ is the ohmic contact resistance.

- Buffer layer spreading resistance, $R_{spreading}$

The buffer layer is a highly doped semiconductor layer. Usually the epi layer semiconductor and buffer layer semiconductors are the same but in this case the layer is a highly doped one. This buffer layer spreading resistance is used to make the current flow possible from the epi-layer to the cathode ohmic contact. The resistance can be expressed as the following according to [14]

$$R_{spreading} = \frac{1}{2Dq\mu_{n,buf}N_{d,buf}}, \quad (2.9)$$

where $\mu_{n,buf}$ and $N_{d,buf}$ are the electron mobility and doping concentration of the buffer layer, respectively. D is the anode contact diameter.

- Junction epi-layer resistance, R_{epi}

Junction epi-layer resistance is the resistance that arises because of the undepleted epi-layer. The conductivity of the epi-layer σ_{epi} is much lower than the conductivity of the buffer layer. It is assumed most of the power is dissipated in the epi-layer and the current

flowing through the diode is concentrated near the anode contact. The epi-layer current spreading resistance can be approximated using the equation

$$R_{epi}(V_j) = \frac{t_{epi} - w_d(V_j)}{Aq\mu_{n,epi}N_{d,epi}}, \quad (2.10)$$

where $\mu_{n,epi}$ and $N_{d,epi}$ are the electron mobility in the epi-layer and donor concentration in the epi-layer, respectively. t_{epi} is the thickness of the epi-layer and $w_d(V_j)$ is the depletion width.

When the diode is forward biased the depletion width $w_d(V_j)$ of the layer decreases with the increase of applied voltage. On the other hand, when the diode is reversed biased the epi-layer can be fully depleted.

- Ohmic contact resistance, $R_{contact}$

Ohmic contact resistance allows current flow between the semiconductor and the external circuit. This contact resistance is usually very low.

2.2 Thermal properties of THz planar Schottky diode

Thermal analysis, one of the key analysis in the field of semiconductor device, is quite popular as it plays an important role in device characterizations. Thermal characterization of a semiconductor device can be considered as determination of the temperature response of the semiconductor circuit junction due to internal self-heating [15]. Much detailed attention in respect of thermal characterization was given to transistors [16, 17, 18]. Thermal characterization of varactors is also reported in [19, 20]. Thermal analysis of the high frequency planar Schottky diode based multiplier chip can be found in [21]. Here the thermal analysis is done for the entire chip not a single anode diode structure. A new method for extracting the series and the thermal resistance can be found in [22].

When the diode is in forward biased condition the heat is generated in the diode because of the current flow through the diode. Most of the power is dissipated in the junction and heat generation occurs. Most of the elevated heat can be found in the top and bottom of the junction. The heat transfer occurs through convection, conduction and radiation. When the diode is only biased with a DC voltage no RF power is delivered, the heat is assumed to be transmitted through convection and conduction in the form of heat transfer in solids. No radiation occurs in this case according to [6]. The dissipation of power in the junction converts into heat energy. As the other layers buffer layer, cathode and anode have high electrical conductivity, most of the power is dissipated in the junction. So the dissipated power P_T can be expressed as

$$P_T = V_j I_d. \quad (2.11)$$

The junction temperature of the diode can be approximated using

$$T_j = T_0 + P_T R_\theta, \quad (2.12)$$

which can be found in [9, 23]. Here T_j is the junction temperature of the diode, T_0 is the ambient temperature and R_θ is thermal resistance.

Thermal resistance in case of a diode can be defined as the temperature difference between the junction, T_j , and another iso-thermal surface, T_x , divided by the power flow, P_T , between them [24]

$$R_\theta = \frac{T_j - T_x}{P_T}. \quad (2.13)$$

For round anodes, thermal resistance can be calculated using the approximate formula in [5]

$$R_\theta = \frac{\rho_\theta}{4r_a}, \quad (2.14)$$

where ρ_θ is the thermal resistivity and r_a is the anode radius.

The thermal problem can also be analyzed by considering only conduction by the following heat equation [25]

$$\rho_m c_p(T) \frac{\partial T(x, y, z, t)}{\partial t} = \{\nabla[\kappa(T)\nabla T(x, y, z, t)]\} + g, \quad (2.15)$$

where ρ_m = material mass density, $c_p(T)$ = thermal capacity or specific heat, $T(x, y, z, t)$ = local temperature, $\kappa(T)$ = material thermal conductivity and g = heat generation per unit volume.

For a steady state case, differential form of Fourier's Law [26] of thermal conduction shows that the local heat flux density \vec{q} is equal to the product of thermal conductivity $\kappa(T)$ and the negative local temperature gradient ∇T

$$\vec{q} = -\kappa(T)\nabla T. \quad (2.16)$$

The heat flux density is the amount of energy that flows through a unit area per unit time.

Thermal conductivity of the semiconductor that is used in the epi and the buffer layer also changes with the temperature. For GaAs the conductivity temperature relationship can be expressed as [27]

$$\kappa_{GaAs}(T) = 50.6 \times \left(\frac{300}{T}\right)^{1.28} \frac{W}{mK}. \quad (2.17)$$

2.3 Different methods for thermal characterization

There are many different ways to measure the temperature within a semiconductor devices. This section covers a few of them and their advantages and disadvantages.

2.3.1 Full wave modeling

The Schottky diode can be modeled using a full wave 3D software like ANSYS mechanical or COMSOL. To model this diode in a 3D simulator first it should be noted if the simulator contains a thermal as well as AC/DC module if only DC simulations are done to characterize the diode. If RF power is also used then it would be better if the software also contains a microwave heating module. In this case, COMSOL was chosen as it contains heat transfer in solids and electric currents module and it is possible to couple these two physics module together. Also it contains microwave heating module which supports the RF heating part, which is not the focus of this thesis. The diode is built to resemble its real life counterpart as accurately as possible. After the geometry is defined, material properties of different layers that have been used in the real life scenario should be associated. Different material properties like thermal conductivity, electrical conductivity, heat density and relative permittivity should be included. The voltage and the ground should also be marked. Now to emulate a real life scenario temperature boundary has to defined and convective cooling from the outside should also be specified. If the doping concentration and mobility of electrons is not known then it is assumed that all the power is dissipated in the epi-layer and the other layers are highly conductive. A full wave model is most efficient as there are no limitation of time and step in this case. In case of time dependent analysis with a very small step size giving rise to the number of steps included in the simulations, simulation time increases. The anode temperature and the heating of different part of the diode can also be seen from these simulations. Any new feature addition is quite simple including the change of outside temperature and effect of convective cooling from outside.

2.3.2 Physical contact method

This method actually uses some other devices that can sense the temperature of the diode or anode junction. Thermocouples, scanning thermal probes, liquid crystals or thermographic phosphorous can be the devices which are used for this purpose. Size of probe or coating particles being used in the measurement determines the spatial resolution and the time response depends upon the thermal response time of the probe or particles [28]. Advantages of the measurement method can be

- They can have a very good spatial response, less than 100 nm.
- Temperature maps can be made from the blanket coating method.

Disadvantages of physical contact method are several. There should be a good surface view of the device and should be available for contacting. Also the method is quite expensive.

2.3.3 Electrical junction temperature measurement

Junction temperature measurement is necessary for realizing the thermal performance of the design and application of the diode. It is widely used nowadays. This method uses the junction temperature as a sensor [24]. The forward voltage drop in the junction is used as a temperature sensitive parameter. Relationship between the voltage drop in the junction and the temperature shows almost a linear relationship when a constant current is applied to the diode. This in turn helps to compute the semiconductor junction temperature in response of the power dissipated in the junction. This current is also known as "sense current" [28]. The constant sense current is small enough not to cause significant self heating. The calibration equation can be expressed as [28]

$$T_j = m * V_F + T_0, \quad (2.18)$$

Where m is the slope, T_0 is the ambient temperature and V_F is the temperature sensitive parameter. V_F is different for each diode. Hence calibration is required for each diode. After calibration the junction can be used as a temperature sensor which is able to measure the temperature using the forward voltage measurement obtained from the sense current.

A known power level is applied to the diode and then switched off to very low value for very short period of time during which the temperature sensitive parameter is measured. This temperature sensitive parameter is compared with the initial value and calibration has been performed in known ambient temperatures. In this method a problem arises with the transient electrical signal. This is very common when switching from high power value to a low power value. The problem can be solved by using a delay. In this time the diode also cools down. The measurement is carried out as soon as the heating signal is interrupted so the diode does not cool down significantly [28].

2.3.4 Liquid crystal imaging method

Liquid crystal is used in the imaging method to evaluate the temperature of the diode. Liquid crystal responds to temperature and this response is used to measure the part of the diode that is coated with liquid crystal. Liquid crystal has a unique property. If the temperature is varied the crystal will reflect visible light of different wavelengths [29]. This is utilized in the imaging method. As the temperature of different parts of the diode is varied different wavelengths of visible light starts to reflect and the temperature variation can be understood from this phenomenon [30].

2.3.5 Method based on S-parameter and temperature controlled measurements

In this method thermal resistance is extracted from temperature controlled I-V measurements at different known temperature and S-parameter measurement at known ambient temperature [22]. The temperature dependent saturation current and ideality factor measurements are verified with the theoretical model in [22]. The S-parameter measurement is carried out in the low frequency and high bias current region. This method describes the effect of self heating of the anode junction on the extracted values of series and thermal resistance.

2.3.6 Pulsed I-V measurements

The traditional DC I-V measurements are found inaccurate for THz Schottky diodes for two reasons, self-heating of the device and trapping effect [31]. Static DC I-V measurements performed at different bias condition can provide good results in cases where self heating of the diode and trapping effect are negligible. For THz Schottky diode the size of the anode junction becomes small. This small anode junction reduces the thermal handling capability of the diode and the effect of self heating becomes significant even for very small currents (in mA). The thermal and trapping effect can change the obtained results found from static DC I-V measurements [32].

To avoid this problem I-V measurement should be done using a very fast signal which is significantly lower than the value of the thermal time constant of the diode. The diode will not be self heated in this case. The diode under test has not time to react thermally. This system provides the capability to make isothermal measurements for such devices where the self-heating of the device can affect the I-V characteristics. In this thesis the simulated results are compared with the pulsed I-V measurement results.

2.4 Analysis for different thermal properties

2.4.1 Steady state thermal analysis

Steady state thermal analysis is done under a condition where the diode is not influenced by the previous temperature of the component. This is done by employing suddenly a constant level of power to the diode and keeping the power constant for a longer period of time. During this time the power dissipation varies which gives rise to temperature. When the temperature is not affected by previous temperature, the temperature becomes stationary and the device reaches its thermal equilibrium. The diode is heated with the voltage for a long time to see the steady state thermal behavior. Theoretically a diode should be heated for an infinite amount of time

to reach its thermal equilibrium. But that is not so in the practical case. During this time the outside temperature and the convective cooling is kept constant. The diode does not go to thermal equilibrium instantly with the introduction of the voltage.

The physical reason behind this phenomenon is the existence of heat capacitance that is present in each matter. These capacitances need to be charged up to go to the thermal equilibrium and charging up via heat flux needs time. When the capacitances are fully charged the diode reaches the steady state condition [24]. As the heat capacitances are a material property, the steady state condition for different diodes of different epi and buffer layer are different. Thermal resistance or impedance can only be computed in the thermal equilibrium with the help of equation (2.13).

Also heating characterization can be found from the steady state analysis. Heating characterization is the response of the diode in a heating condition. It contains a complete behavior of the diode ranging from transient to steady state. This data are very helpful for analyzing and predicting the behavior of the diode in different power conditions [24].

2.4.2 Transient thermal analysis

This type of thermal analysis is employed to define the transient thermal properties shown by the diode. The thermal time constant can be found out using the transient thermal analysis. A small pulse voltage is used and the diode is let to cool down after the pulse. The diode temperature does not abruptly fall down. Some time is needed for the diode to completely come to the ambient temperature. The thermal time constant can be found out from the following formula.

$$T_j = P_T R_{\theta} \left[\frac{4}{\pi^2} \right] \left[\frac{t}{\tau} \right]^{\frac{1}{2}} \quad (2.19)$$

for $t < \tau$. Here, τ = thermal time constant and t = time.

This equation is found to be accurate during the early part of the pulse not the entire duration of the pulse which is further described in [33].

The thermal time constant can be also estimated using

$$\tau = \left[\frac{2F}{\pi} \right]^2 \left[\frac{\rho C_p}{\kappa} \right], \quad (2.20)$$

according to [33]. Here F = die thickness.

The thermal time constants are found out in this thesis by heating the diode for a very long period of time and fitting the variation of temperature with time in and find out the different time constants. If the rise time of the diode has to be fitted the following equation can be used.

$$T = T_0 + T_1 \times \left(1 - \exp\left(\frac{-t}{\tau_1}\right) \right) \quad (2.21)$$

where T_0 is the ambient temperature, T_1 is the temperature coefficient and τ_1 is the thermal time constant. The temperature rise vs time curve of the diode can be fitted with several time constants using MATLAB.

Chapter 3

Modeling and analysis methodology

The Schottky diode can be modeled using full wave 3D software like ANSYS mechanical, CST Studio Suite and COMSOL Multiphysics. To model a diode in a 3D simulator it should be first noted if the simulator contains a thermal as well as electrical current module to perform DC simulations of the diode. COMSOL Multiphysics has a good coupling between different physics phenomena like heat transfer and electrical currents. Also there is a separate module called joule heating which is a coupled physics module, providing coupling between electric currents and heat transfer [34].

If RF heating is considered, there is a separate module to use as well. The diode is built to resemble its real life counterpart as accurately as possible. After the geometry is defined, material properties of different layers that have been used in the real life scenario should be associated with the model. Different material properties such as thermal conductivity, electrical conductivity, heat capacity, and relative permittivity should be included. The voltage and the ground should also be marked. To emulate a real life scenario temperature boundary has to be defined which represents the flow of heat away from the diode. If the diode is cooled down by external cooling mechanism, it can also be simulated using a convective cooling mechanism.

3.1 Modeling of a simple diode

A simple diode which is called as test diode A for the rest of the thesis is approached at first. This diode contains only the basic layers an anode, a cathode, an epilayer and a buffer layer. The resistance of each layer can be found from the resistance definition formula

$$R = \rho \frac{L}{A}, \quad (3.1)$$

where ρ is the resistivity of the material and L and A are the length and area of the layer, respectively.

Stationary and time dependent simulations have been performed for test diode A. The maximum temperature of the junction, thermal resistance and the thermal time constants can be found from these simulations. Structural dimensions of different layers can be found in Table 3.1.

Table 3.1: Structural parameters of different layers of test diode A

Layer	Material	Radius (μm) or length (μm)	Height (μm)	Width (μm)
Anode Extended	Gold	2	2	
Anode contact	Gold	0.4	0.6	
Anode finger	Gold	20	2	4
Buffer layer	GaAs	7.51	2	
Epilayer	GaAs	0.6	0.05	
Insulating layer	SiO ₂	7.51	0.6	

The structure of test diode A can be found in Figure 3.1. In a Schottky diode almost all the power is dissipated in the epilayer. The buffer layer is much more conductive than the epilayer.

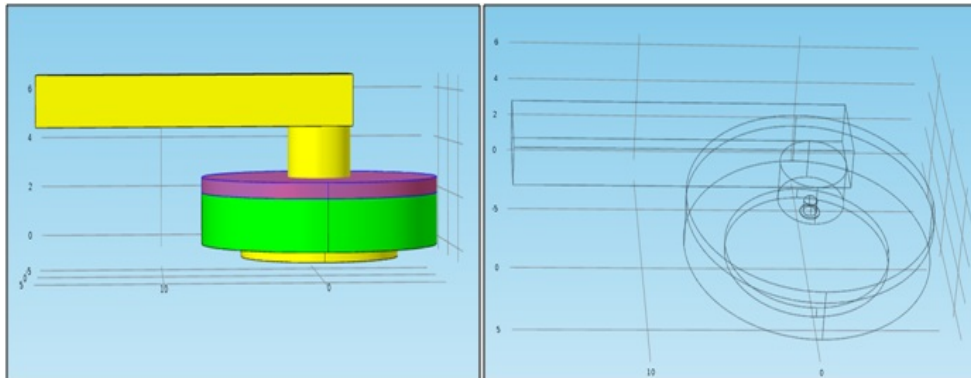


Figure 3.1: Test diode A containing all the basic layers (anode, cathode, insulation, buffer, epi layer) (left); wire frame view of the diode (right).

The material properties that are used in the simulations can be found in Table 3.2. Here the electrical conductivity that is mentioned in Table 3.2 is not the actual epilayer conductivity. The epilayer here is working as a resistor to have the desired amount of current flow through the diode or diode current and the electrical conductivity of the epilayer is changed to achieve that amount of current.

Table 3.2: Material properties of different layers of diode model test diode A

Material	Thermal conductivity(W/mK)	Specific heat capacity (J/kgK)	Mass density (kg/m ³)	Electrical conductivity (S/m)	Relative permittivity
Epi layer GaAs	51 × (300/T) ^{1.28}	327	5317	830	12
Buffer layer GaAs	51 × (300/T) ^{1.28}	327	5317	4.1 × 10 ⁷	12
Gold	310	130	19320	4.1 × 10 ⁷	1
SiO ₂	1.4	730	2200	0.01	4.2

3.2 Modeling with only heat transfer

One simple method to tackle the problem in hand is to only treat the problem as a thermal problem. It is evident that almost all the power is dissipated in the epilayer. So if a heat source can be specified in the anode junction the thermal problem can be solved. The thermal parameters that can be found in Table 3.2 are responsible for the conduction of heat and that is why we can have different temperature in different parts of the diode. The specific heat capacity or material heat capacitance is responsible for the transient thermal behavior of the diode. The amount of power that we want to use can be described as a heat source and it should be specified in the epilayer. One drawback of this method is the diode current cannot be found. The current change that happens with the rising temperature cannot be found while using this method of simulation. While using this method the power is kept constant. This constant power is conducting heat through the entire diode. But for different heating time it is later shown that we have different temperature. This phenomenon happens because of Joule's law.

Joule's law states the heat energy produced in a conductor is dependent upon the current passing through the conductor, the resistance of the conductor and time of power supplied.

$$Q = I^2 R t, \quad (3.2)$$

where Q is the heat energy produced by a constant current I through a conductor with resistance R for a time t .

3.3 Modeling with heat transfer and electric currents

As most of the power is dissipated in the epilayer, the buffer layer is assumed to be electrically very conductive and the insulating layer is much less conductive. Almost no current passes through the insulating layer and for this reason there is almost no heat dissipated in the insulating layers. The heat generation can be stated in the following manner:

$$Q \propto I^2 R, \quad (3.3)$$

where Q is the amount of heat energy produced. I and R are the current passing through each layer and resistance of each layer, respectively. This heat energy produced will eventually give rise to the temperature. If the current and the corresponding voltage of the diode is known, the resistance of each layer (except the epilayer) can be found out using the resistance formula and the epi layer resistance can be found out using Kirchoff's voltage law, as the voltage and current is known. If the resistance of the epilayer is known then electrical conductivity can be easily derived from that. When the diode structure is complex then the resistance formula is very difficult to use and at that time the conductivity of the epilayer can also be established by trial and error basis. Once again, the electrical conductivity of the epilayer here is not the actual conductivity of the epilayer of the diode. It works as a resistor which can dissipate a fixed amount of power in the epilayer.

3.4 Modeling with COMSOL Multiphysics

In COMSOL Multiphysics a common way of modeling is maintained. First the geometry of the diode is drawn as accurately as possible to resemble its real life counterpart. The diode model can also be imported from any 3D cad software using .step format. The materials have to be defined. Meshing plays a very important role in the simulations. Meshing size in different parts should be defined as different increments of meshing increase the number of degrees of freedom in the simulations and which eventually increases the simulation time. Meshing size decrease in an area increases the accuracy of the simulations. Increment of number of degrees of freedom to be solved and increment of simulation time can be evident from tables found in the results and analysis chapter.

In COMSOL it is possible to couple two different physics module and in this case the heat transfer in solids and electric currents module have been coupled with each other. The electric current passing through the diode will give rise to heat and that will increase the temperature. Some simulations are also done using only heat transfer in solids module in COMSOL. In the latter cases the epilayer is selected as a heat source and the heat is transmitted throughout the diode through the conduction heat and this increases the temperature. As it is later shown in the

thesis while using only heat transfer in solids module in COMSOL less junction temperature was found compared to when heat transfer in solids and electric currents module coupled together. A reason behind this can be while using the heat transfer in solids module the diode current cannot be found but when using the coupling between the heat transfer in solids module and electric current module the exact diode current can be found by integrating the current density of the cathode surface. The electrical parameters that are used for different materials in this thesis is changed in such a way that the desired amount of current is dissipated in the epilayer. These parameters are not actual electrical parameters and they can be responsible for the difference between the temperature found from the two methods used in the thesis.

In the anode portion of the diode, a terminal boundary has been defined as an electric potential to emulate the applied voltage in the diode in real life scenario. The ground is set to be in the outer side of the cathode boundary. The current will flow among all the layers of the diode and that will cause the heat generation in the diode.

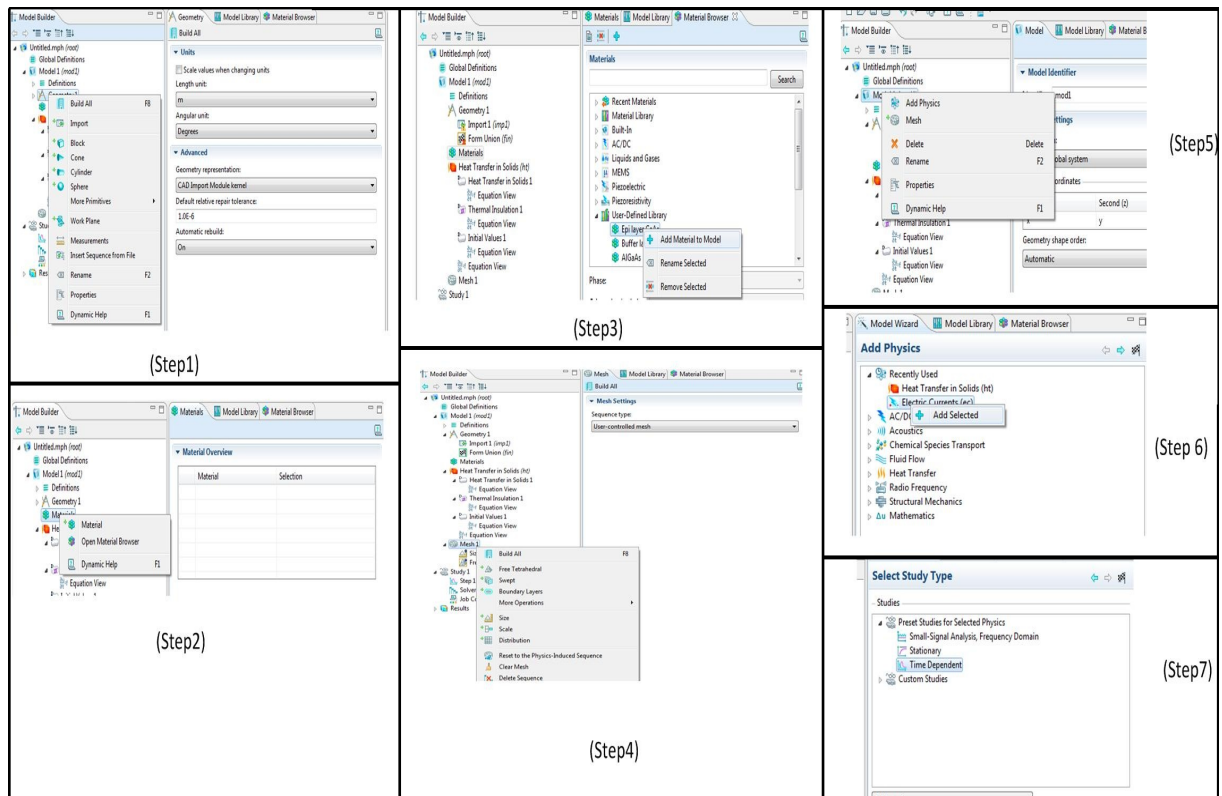


Figure 3.2: Modeling with COMSOL. 1st: import geometry, 2nd: adding material, 3rd: adding material to different layer of the model, 4th: defining mesh for different layers of the model, 5th: adding physics, 6th: defining physics in the model, 7th: adding solvers.

Current passing through the diode can be found by integrating the current density in the outer cathode/ground surface. The current has been controlled by changing the conductivity of the epilayer. The epilayer conductivity has been first found from doing the calculation by hand, using Kirchoff's voltage law. The voltage supplied to the anode is known and the current that flows through the diode is desired. For more complicated structure the current can be found by

changing the epilayer conductivity using trial and error basis.

A pictorial view is presented from geometry import to the physics setup option. The different steps to be taken in COMSOL modeling can be found in the Figure 3.2. The diode should have a temperature boundary defined. This temperature boundary will eventually represent the heat flowing away from the diode and the temperature there should be the outside temperature. The ambient temperature can be changed to see the diode operating in different temperatures.

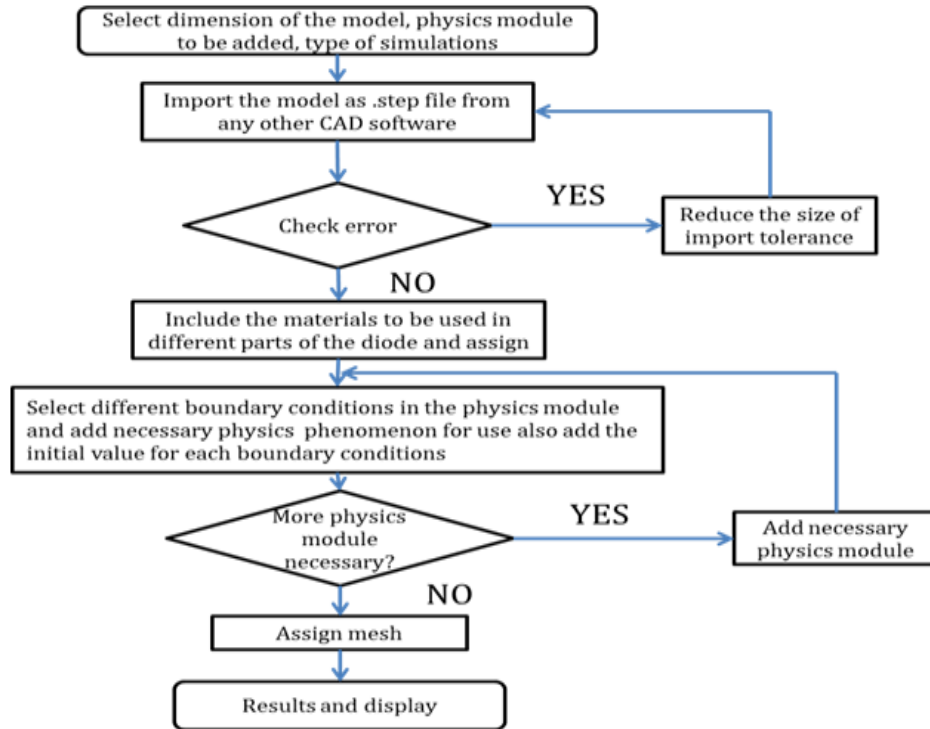


Figure 3.3: Flowchart representing process for COMSOL modeling.

To find out different thermal parameters different simulations are used. The junction temperature of the diode and temperature distribution of the diode can be done using the stationary simulations but to get the thermal time constants time dependent simulations have been applied. This process works accurate for constant voltages. For different applied voltages this process also can be used by applying different amount of voltages and changing the epilayer conductivity each time to get the amount of current desired. This is a very time consuming process. A smart way of modeling the diode with different applied voltage is to include the diode current-voltage relationship equation (2.4) in COMSOL. The saturation current and ideality factor of the diode should be known exactly while using this process.

When the diode parameters such as saturation current and ideality factor are known the diode I-V curve can be found by incorporating equation (2.4) in COMSOL. The diode current can be simulated and from the current and voltage, the changing conductivity with the change of

Name	Expression	Value	Description
Isat	0.15e-15	1.5000E-16	
q	1.602e-19	1.6020E-19	
kB	1.38e-23	1.3800E-23	
n	1.27	1.2700	
eps	1e-50	1.0000E-50	

Figure 3.4: Assumed diode parameters for test diode A.

applied voltage can be modeled using equation (3.1).

Name	Expression	Unit	Descrpt
Tj	maxop1(T)	K	
I	Isat*exp((q*v)/(n*kB*Tj))		
v	rect1(tL/g)		
sigma_epi	(7*0.05e-6)/(v*pi*0.05e-6^2)		

Figure 3.5: Process to find out junction temperature(left). Incorporating current-voltage relationship in COMSOL (right).

Figure 3.5 shows the process which shows the parameter entry and incorporating I-V relationship in COMSOL. If only heat transfer is used then there is no need of coupling between the physics modules. Heat transfer is the primary objective and the results can be found by defining the heat transfer module. The temperature boundary and other parts remain the same as before.

If the electrical conductivity and the mobility of particles in each layer is known then it is also possible to simulate the diode using a separate physics module that is included in COMSOL Multiphysics called transport of diluted species. Using this physics module it is possible to simulate the transport phenomenon in a semiconductor. But to use this physics module much knowledge in semiconductor physics is required also parameters such as electron mobility, drift velocity and electrical conductivity of both epilayer and buffer layer has to be known. This parameters are kept secret by the manufacturers of the diode and are not easy to come by. That is why this physics module is not used in this thesis.

Chapter 4

Results and discussions

In this chapter results are described, presented and analyzed for three separate diode models. One was the simple diode model which is known as test diode A. The other two are commercial diodes. From those, one is a mixer diode from ACST GmbH which is referred as test diode B and the other is a varactor diode from Chalmers University of Technology which is referred as test diode C for the rest of the thesis. The maximum temperature of the junction, thermal resistance and the thermal time constants can be found from these simulations.

4.1 Temperature distribution on diode surface

First the diode, test diode A was simulated using a stationary solver. The structural and the material parameters that are included in the model can be found in Chapter 3 in Table 3.1 and in Table 3.2, respectively. Free meshing was used in this case. Free meshing is actually the meshing that is done by COMSOL automatically if no meshing is defined. The voltage supplied was 1 V. The epilayer conductivity was changed in such a way that the current found after integrating the current density over surface of the cathode was 5 mA. All these simulations were done at ambient temperature 293.15 K.

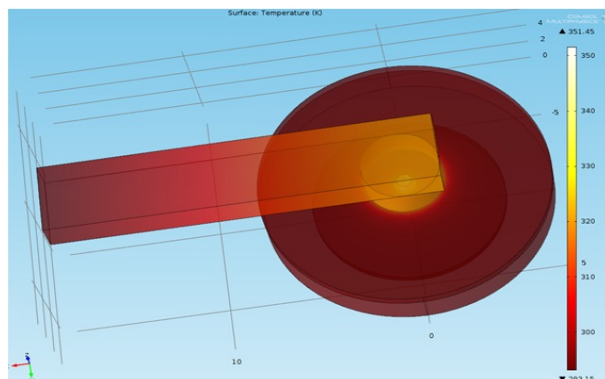


Figure 4.1: Temperature distribution on the surface of test diode A (current 5 mA and voltage 1 V).

A more detailed picture of temperature distribution is shown in Figure 4.2 and Figure 4.3. The diode has been split in the XZ plane and the cross section of the diode can be seen in Figure 4.2.

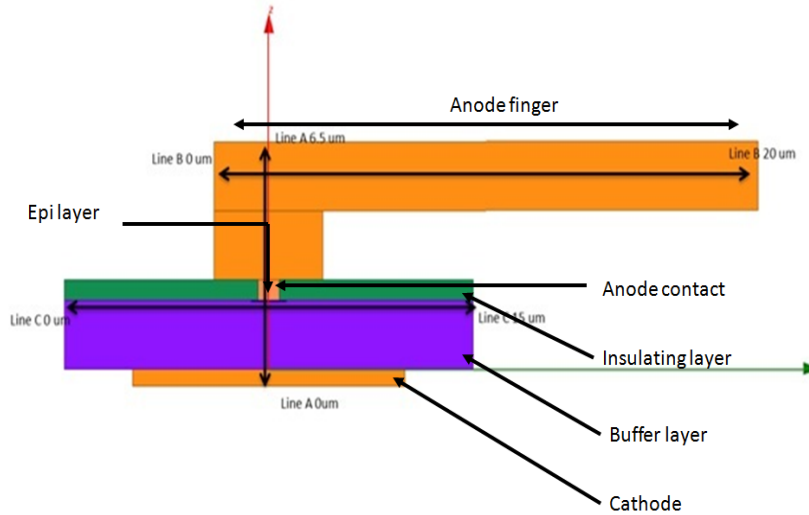


Figure 4.2: Cross section of the simple diode split in XZ plane with different lines of measurement of temperature.

The temperature calculated from equations (2.14) and (2.12) was found to be 362.5 K. So the temperature difference between the theoretical and the simulated result was found to be around 8 to 9 K. This temperature difference is the result of the anode and the other parts of the diode which takes much of the heat away from the junction.

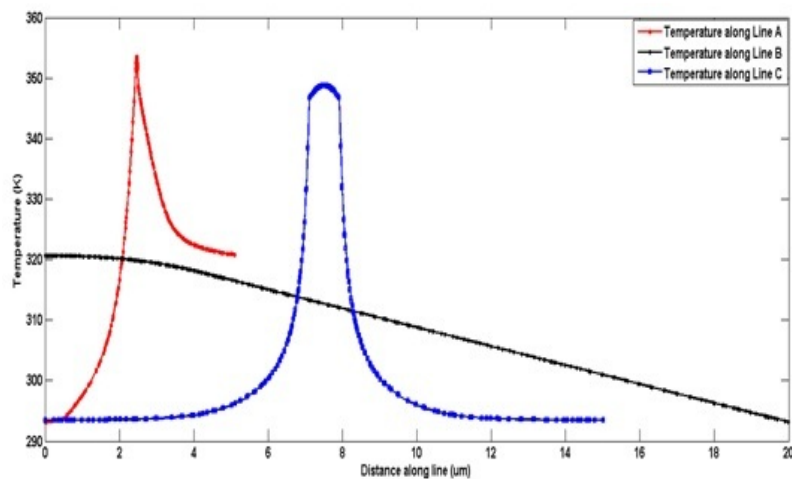


Figure 4.3: Temperature distribution along different lines described in Figure 4.2 for 5 mW input power.

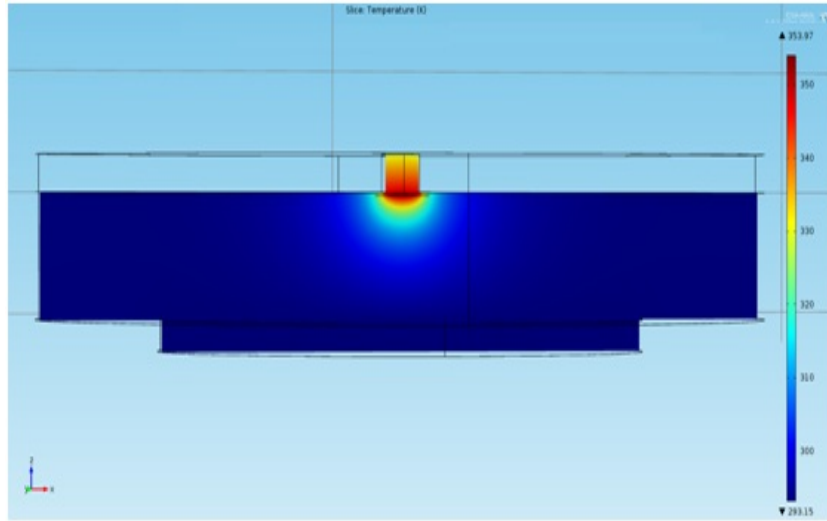


Figure 4.4: Slice of the diode for temperature distribution in XZ plane with 5 mW input power.

Figure 4.4 represents a slice of test diode A in XZ plane. Here the junction temperature was 353.96 K. The main focus of this figure is the junction temperature and how the heat flows from the junction. The temperature distribution in the insulating layer SiO_2 is not shown here. Some heat also flows away from the insulating layer.

To find out the difference between the calculated junction temperature using equations (2.14) and (2.12) and the simulated junction temperature a simple structure was developed which had only a buffer layer, an epilayer, an anode and a cathode with the structural properties found in Table 4.1.

Table 4.1: Structural parameters of a simple structure to find out the heat loss

Buffer layer radius (μm)	Buffer layer height (μm)	Anode height (μm)	Anode radius (μm)
7.51	1	0.1	0.5

A simple structure with the structural parameters found in Table 4.1 and shown in Figure 4.5 has been presented to find out the power loss in a diode structure. 10 mA current and voltage 1 V is used for this purpose.

The temperature calculated from equation (2.14) and (2.12) was found to be 408.1 K. Here the thermal conductivity used for the epilayer and buffer layer thermal conductivity as 45 ($\text{W}/\text{m K}$) for the ease of calculation. The ambient temperature was kept at 295.15 K.

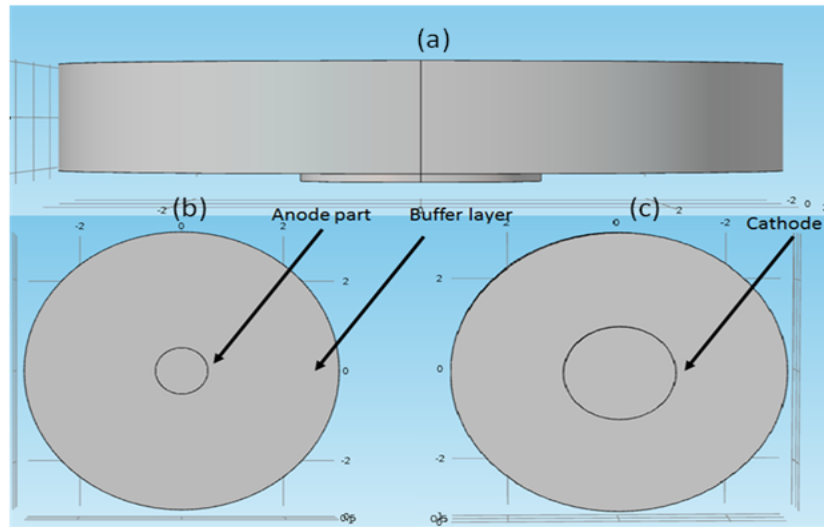


Figure 4.5: Simple structure model to find out the temperature loss. (a) Side view of the simple structure, (b) top view of the structure and (c) back view of the structure.

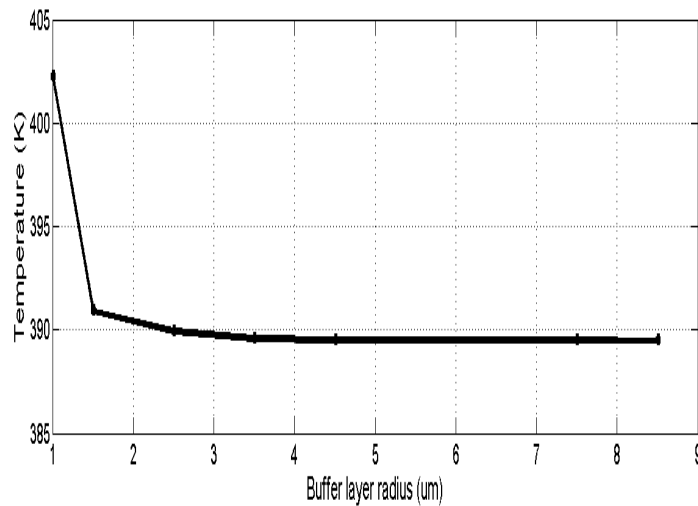


Figure 4.6: Variation of junction temperature with buffer layer radius for the simple structure with 1 V and 10 mA.

At first the buffer layer radius was decreased and the junction temperature increased with the decrease of buffer layer according to Figure 4.6. The highest junction temperature was achieved when the buffer layer radius was $1.01 \mu\text{m}$. This highest junction temperature was found at 404.1 K. Still there was a 6 K difference between the theoretical and simulated results. So the buffer layer radius was kept constant at $1.01 \mu\text{m}$ and the anode height was decreased. When the anode height was decreased the junction temperature increased which is presented in Figure 4.7. The highest temperature achieved was 407.1 K. As the anode height is increased, the amount of conductive material increases and this takes away heat from the junction. So the junction temperature decreases with the increment of the height of the anode.

Also to minimize this temperature difference, meshing has been increased. As it was discussed in Chapter 3, the number of degrees of freedom increases with the decremented of meshing size,

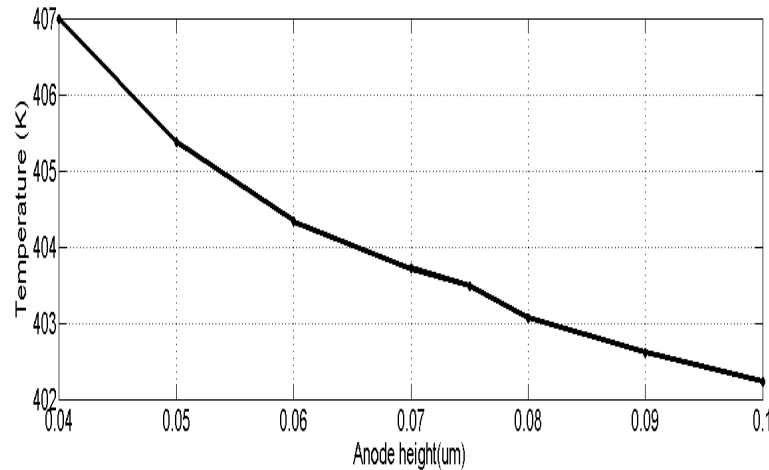


Figure 4.7: Variation of junction temperature with anode height for the simple structure with 1 V and 10 mA.

the simulation time also increases. Table 4.2 and Table 4.3 represent the effect of increment of degrees of freedom to the simulation time. The computer that has been used for this simulation purpose has four CPUs and 4 GB of memory. This does not have that much large effect in stationary simulations but in time dependent cases this issue affects a lot.

Table 4.2: Effects of degrees of freedom to be solved in simulation time for voltage of 1 V and current of 5 mA

Number of degrees of freedom to be solved	Simulation time (s)	Junction temperature (K)
410882	33	353.96
143140	12	353.02
69314	7	353.57
37250	5	353.27
25094	4	352.45

Again the diode was supplied with 1 V and the current that was desired is 1 mA. The epilayer conductivity is varied in such a way that the total diode current is kept at the desired current. Here the temperature rise according to equation (2.14) and (2.12) should be 13.75 K and the junction temperature should be at 308.37 K. So there is a difference between the calculated and simulated junction temperature of 1 to 2 K.

Temperature distribution of test diode C, which was a varactor diode and provided by Chalmers University of Technology, was also seen. Here the diode was mounted in a quartz carrier in two different configurations. The configurations are on wafer CPW and metal housing made of brass

Table 4.3: Effects of degrees of freedom to be solved in simulation time for voltage of 1 V and current of 1 mA

Number of degrees of freedom to be solved	Simulation time (s)	Junction temperature (K)
410882	22	308.35
149112	10	308.36
143410	9	308.36
65034	5	308.37
63398	5	308.37

configurations. The ambient temperature was kept at 295.15 K. Two methods of simulations, one using only heat transfer in solids and the other one using heat transfer in solids coupled with electric currents module in COMSOL Multiphysics were used to find out the difference in the results. The thermal properties of the materials used in these simulations can be found in Table 4.4. Electrical properties of the material was changed in such a way that the desired amount of power 10 mW in this case was dissipated in the epilayer of the diode.

Table 4.4: Material properties of different layers of diode model test diode C

Material	Thermal conductivity (W/m K)	Specific heat capacity (J/kg K)	Mass density (kg/m ³)
GaAs	$51 * (300/T)^{1.28}$	327	5317
Gold	310	130	19320
Quartz	1.3	670	2200
Solder	43	243	7850
Brass	109	377	8600

To have a better understanding of the temperature distribution of the test diode C, temperature along the line in the Figure 4.8 has been provided. The diode is cut into half, attributed to the symmetrical property of the structure.

From Figure 4.9 it can be depicted that the air bridge finger is heated up more compared to the other regions. Also the diode in metal housing exhibited higher temperature than the CPW configurations. Also the simulations that involved both the heat transfer and electric currents physics module presented a slightly higher temperature. The difference between results of the two

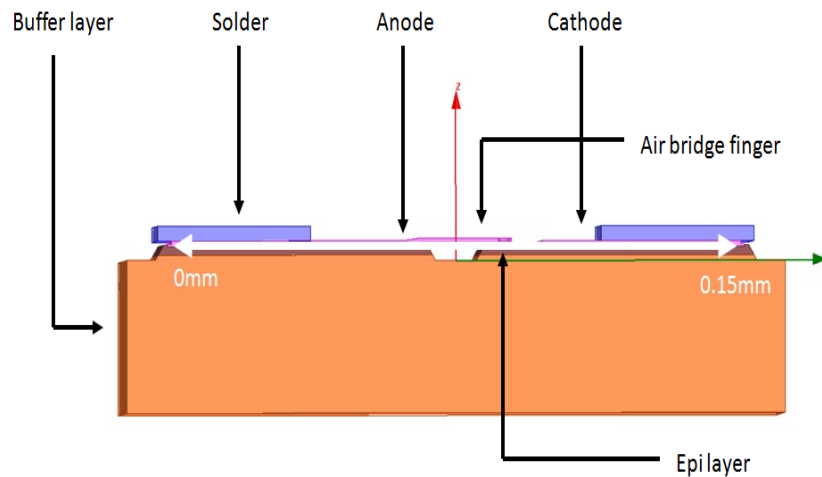


Figure 4.8: Cross section of test diode C split into half in XZ plane with lines of measurement of temperature.

methods of simulation was found to be 4-5 K. The reason behind this can be the electric currents cannot be found when the diode is simulated using only heat transfer in solids physics module. So the current in this case can be lower than the current that is found out and kept constant when heat transfer and electric current module are coupled together. This lower current can be the result of low junction temperature. The metal housing configuration simulations exhibits more junction temperature because the temperature boundary is further away from the junction, which enables the junction temperature to be a little more than the CPW configurations. The outer part of the metal housing was selected to be the temperature boundary when using this metal housing configuration and the outer part of the quartz substrate was selected to be the temperature boundary in CPW configurations.

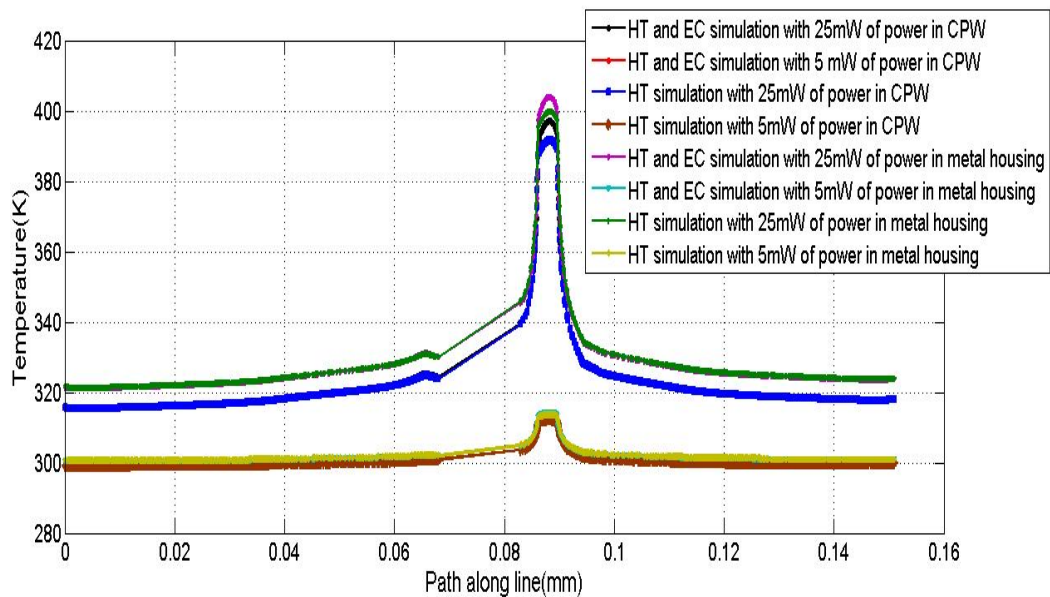


Figure 4.9: Temperature distribution of test diode C along the line described in Figure 4.8.

The highest temperature was found when both electric currents and heat transfer module was used and the diode was in metal housing configuration. For 25 mW of power dissipation the temperature found was 404 K and the highest temperature was found in the middle of the anode junction. All the simulations using both methods and both configuration for 25 mW of power the junction temperature was found in the region of 391-404 K.

For 5 mW of power the temperature found using both simulation methods and both configurations was from 312.3-314.4 K. The highest temperature was found when using both electrical currents and heat transfer in solids module coupled together and in the metal housing configuration.

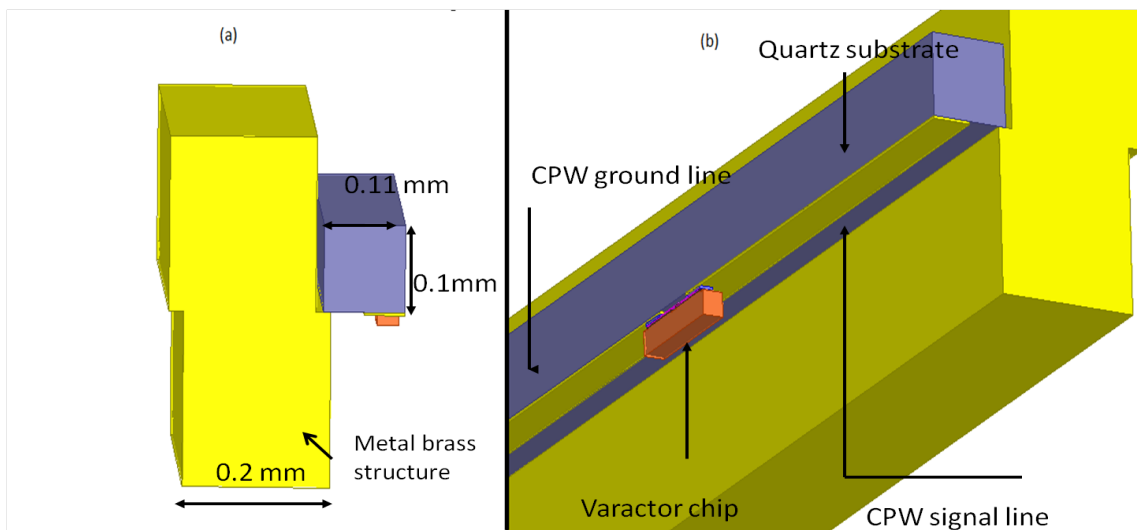


Figure 4.10: Metal housing structure with dimensions.

The metal housing structure with dimensions are presented in Figure 4.10 and Figure 4.11. In these figures only half of the diode is presented. Because of the symmetry of the structure the other half of the diode would be the same.

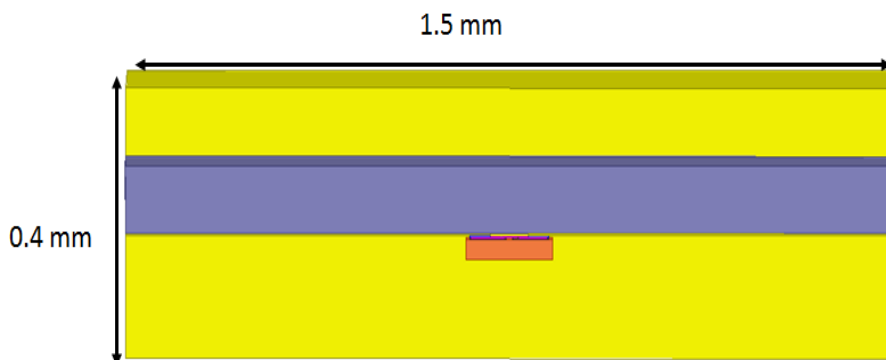


Figure 4.11: Metal housing structure with dimensions.

4.2 Simulations related to thermal resistance

Thermal resistance can be calculated using equation 2.13. Another diode which was a mixer diode and referred as test diode B, provided by ACST GmbH has been used for this measurement. This diode structure was mounted on quartz substrate. The material properties of test diode B can be found in Table 4.5. The structure of the diode was a bit similar to that of the test diode A.

Table 4.5: Material properties of different layers of diode model test diode B

Material	Thermal conductivity (W/m K)	Specific heat capacity (J/kg K)	Mass density (kg/m ³)
GaAs	$51(300/T)^{1.28}$	327	5317
Gold	310	130	19320
Quartz	1.3	670	2200
SiO ²	1.4	730	2200
AlGaAs	78.68	342	5320

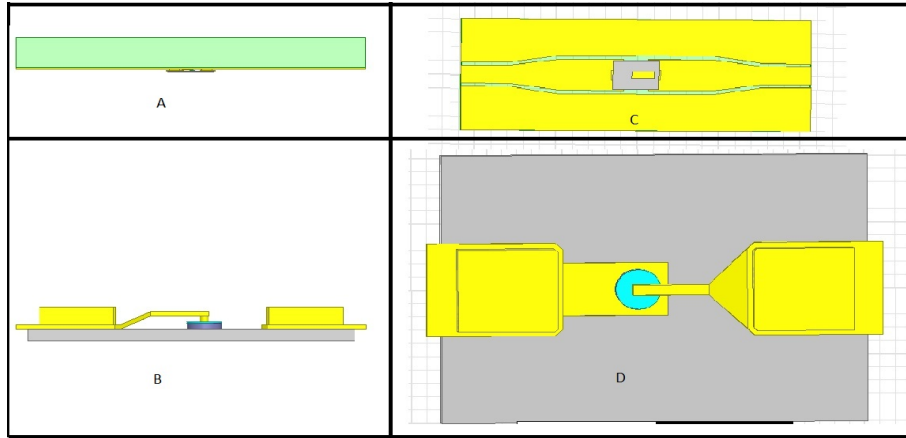


Figure 4.12: Structure of test diode B. A: Side view of the diode under quartz. B: Side view of the diode. C: Top view of the diode mounted on quartz. D: Top view of the diode.

The radius of the anode was $0.5 \mu\text{m}$. The anode radius was changed to find out different thermal behavior of the same diode with different anode size. The ambient temperature was kept fixed at 295.15 K. First power at anode was swept from 5 mW to 25 mW at the interval of 2.5 mW. Anode radius of the diode was changed to $0.4 \mu\text{m}$ and $0.6 \mu\text{m}$ to see the variation when the anode radius was changed. Theoretically the junction temperature should be a lot more according to equation (2.14) and (2.12) at 25 mW when the anode radius was $0.4 \mu\text{m}$ than when anode radius was $0.5 \mu\text{m}$ and $0.6 \mu\text{m}$.

The difference between the junction temperature of the changed anodes varies more when the

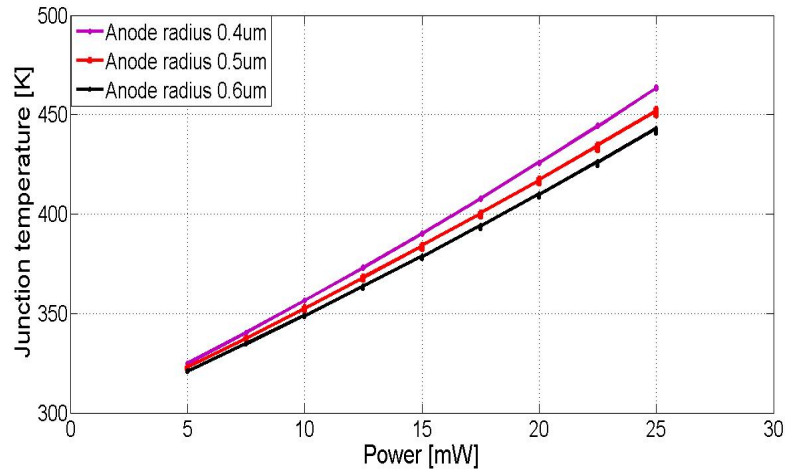


Figure 4.13: Junction temperature with variation of power for test diode B.

power is high than in low power such as 5 mW. Junction temperature variation while using 5 mW of power between the highest junction temperature (of 0.4 μm radius anode) and the lowest junction temperature (of 0.6 μm radius anode) was found only 3.7 K whereas when 25 mW of power was used the junction temperature difference between these two (463.7 K - 441.7 K) was 22 K.

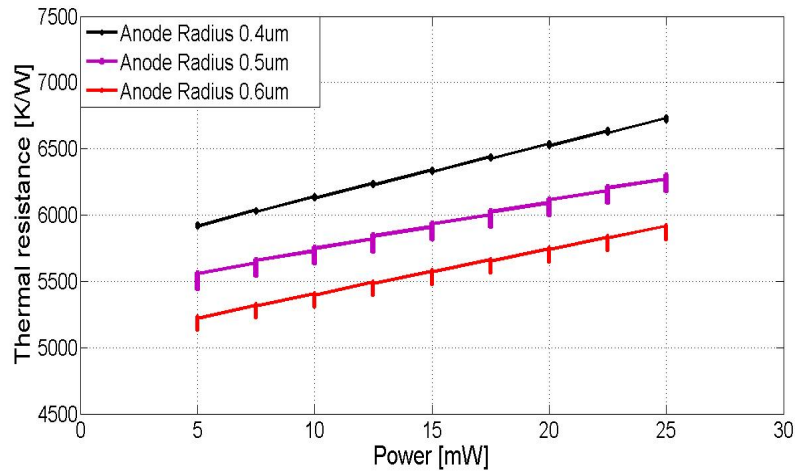


Figure 4.14: Thermal resistance with the variation of power for test diode B.

The measurement of thermal impedance can be done from this simulation using equation (2.13). The thermal resistances were found within the range of 5.5×10^3 - 6.2×10^3 K/W for the test diode B with anode radius 0.5 μm .

Same simulations was done for test diode C. Again two methods were applied. The first one with only heat transfer in solids physics module and the other one with heat transfer in solids and electric current module in COMSOL coupled together. Test diode C has been also simulated in two configurations: one using co-planar waveguide configuration, the other one using a metal block made of brass. As results in Figure 4.16 indicate the highest temperature was found using the metal block configuration and when using heat transfer and electric currents coupled together. The lowest temperature was found using the CPW configuration and only using the

heat transfer in solids module. The junction temperature at 25 mW varied from 391-404 K. The diodes in metal housing exhibited higher temperature and higher thermal resistance compared to the diodes in CPW configuration. Thermal resistance of the diode in metal housing has been found in between 3.8×10^3 - 4.4×10^3 K/W whereas the thermal resistances found for the CPW configuration and using only heat transfer was found in the range of 3.4×10^3 - 3.9×10^3 K/W. The thermal resistances were obtained using equation (2.13) .

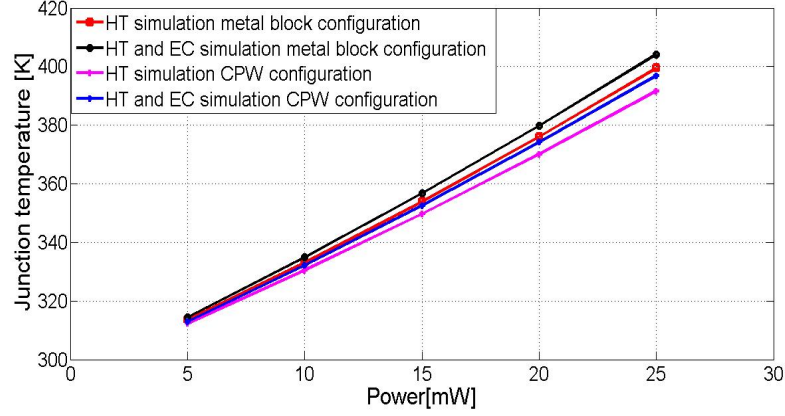


Figure 4.15: Junction temperature with variation of power for test diode C.

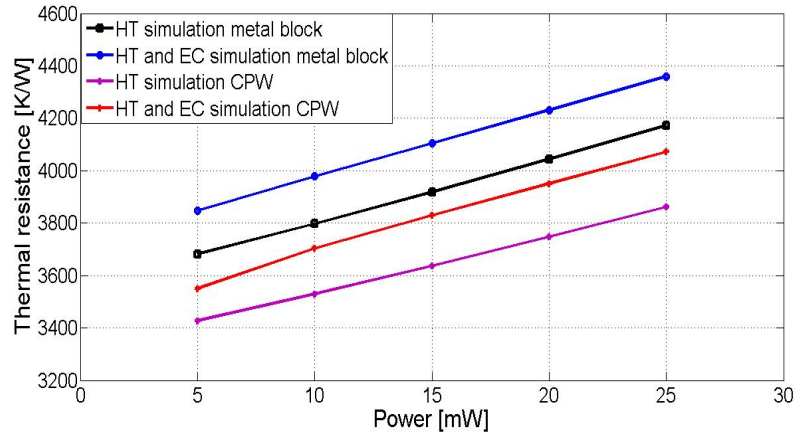


Figure 4.16: Thermal resistance with the variation of power for test diode C.

4.3 Variation of the epilayer

The epilayer is actually a single crystal layer that is formed on the top of a single crystal substrate. An epitaxial layer will normally have a lower electrical conductivity than the buffer layer.

In this thesis the epilayer is considered as a cylindrical structure for the ease of the simulation. But practically the situation is not like that. So it is necessary to study the cylinder height and radius variation to validate the study. To study this phenomenon a voltage pulse was sent with $1 \mu\text{s}$ of pulse length and a delay of 10 ns. The pulse voltage had an amplitude of 1 V. Figure

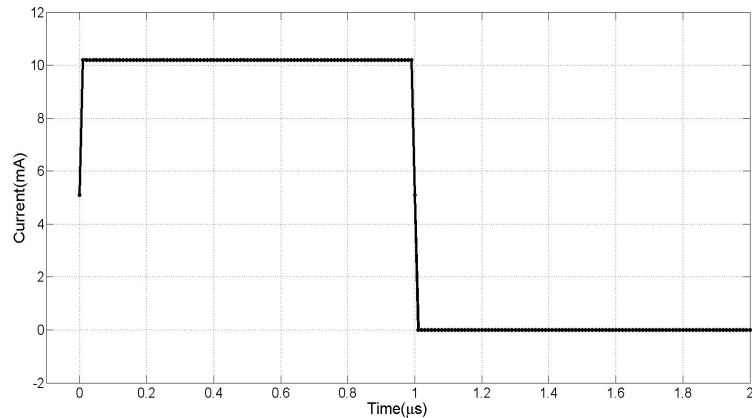


Figure 4.17: Diode current with time while using 1 V and epilayer resistance changed to get 10 mA current.

4.17 reflects the diode current after integration of current density has been done in the cathode area of the diode on the surface of the cathode. The current desired was 10 mA after tuning the epilayer electrical conductivity.

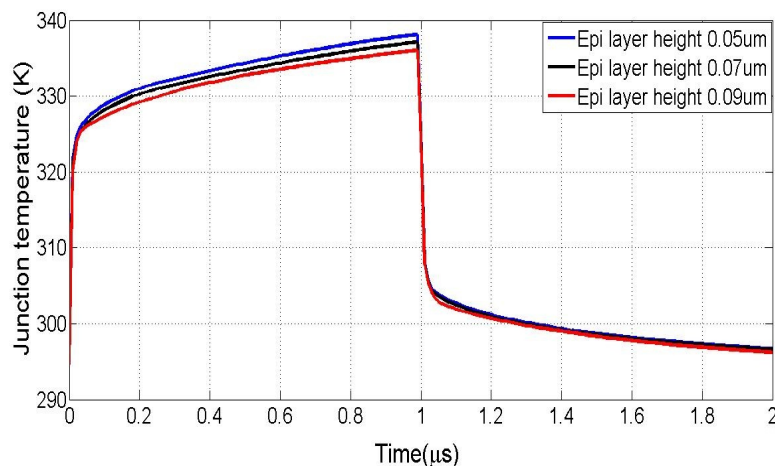


Figure 4.18: Test diode A temperature vs time with the variation of epilayer height with voltage 1 V, current 10 mA, and 1 μ s pulse length.

Figure 4.18 shows a figure of test diode A with varying epilayer height. The initial height was 0.05 μ m. The height was changed to 0.07 μ m and 0.09 μ m. It showed the temperature variation in varying the height of the cylindrical epilayer is only 1 K.

Again this same simulation was done using test diode B. Here the original height was created as 0.06 μ m and then varied to 0.08 μ m and 0.1 μ m. Here also the temperature drops 1 K with the change of epilayer height. It can be noted as the epilayer height increases the temperature falls down. In all used cases the current was kept constant at 10 mA.

The radius of the cylinder was also varied. In this case the test diode A was taken into account. The initial radius was 0.5 μ m. The radius has been changed from 0.5 to 0.7 μ m. The variation

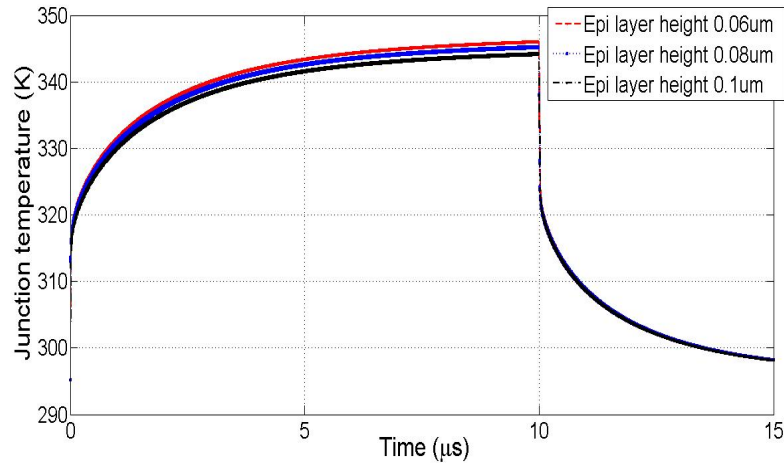


Figure 4.19: Test diode B temperature vs time with the variation of epilayer height with voltage 1 V, current 10 mA, and 1 μ s pulse length.

found in the temperature is less than 1 K according to Figure 4.20.

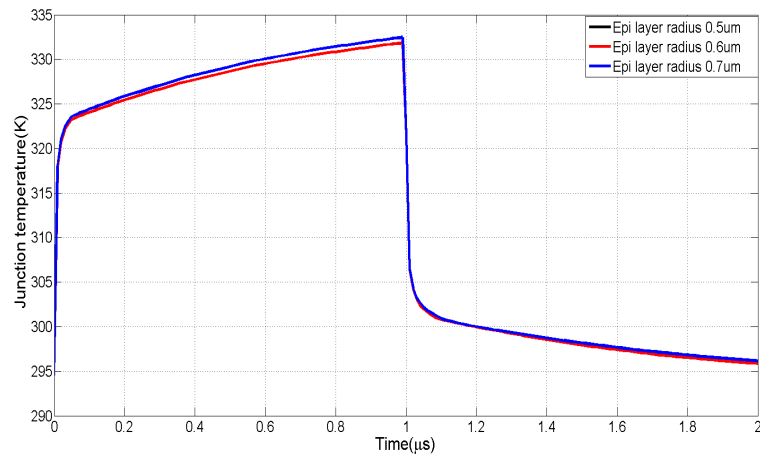


Figure 4.20: Test diode A temperature vs time with the variation of epilayer radius with voltage 1 V, current 10 mA, and 1 μ s pulse length.

In this case also a pulsed voltage of 1 μ s and 10 ns fall time was given as an input and the voltage amplitude was set at 1 V. The current was changed by changing the epi layer electrical conductivity in such a way that it keeps constant 10 mA when the voltage was 1 V.

4.4 Variation in anode finger

The temperature boundary is found to be an important concept as it represents where the heat will finally flow away from. The temperature boundary actually resembles a highly thermally conductive region. This boundary has to be set to a right place or else the temperature of the junction of the diode will vary. To check how the temperature boundary changes the diode junction temperature again a voltage pulse of 1 μ s with a fall and rise time of 10 ns was applied.

The voltage amplitude was set to 1 V.

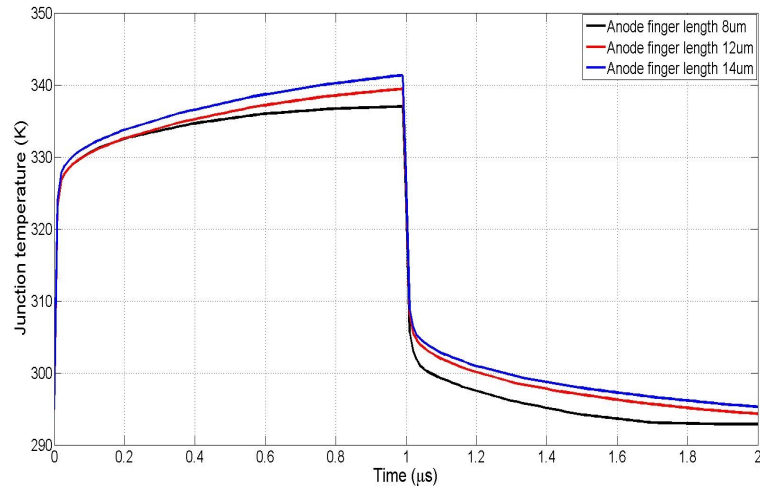


Figure 4.21: Test diode A temperature vs time with the variation of anode finger length with voltage 1 V, current 10 mA, and 1 μ s pulse length.

Test diode A was simulated to portray the fluctuation of junction temperature with the variation of the anode finger length. The temperature boundary was set at the tip of the anode finger and the temperature there was set to be the ambient temperature 293.15 K in this case. The diode current is kept constant at 10 mA when the voltage is 1 V by changing the conductivity of the epilayer. As the temperature boundary is further away from the junction of the anode the temperature will continue to rise. To find out the variation of temperature by varying the anode finger length the length of the anode finger was changed from 8 μ m to 12 μ m. Figure 4.21 shows the variation of temperature with the varying anode finger length. The junction temperature when the finger length was 8 μ m was found to be around 337 K and when it is changed to 14 μ m the temperature was found around 342 K. There is almost a 5 K rise of temperature when the anode finger is only 6 μ m longer.

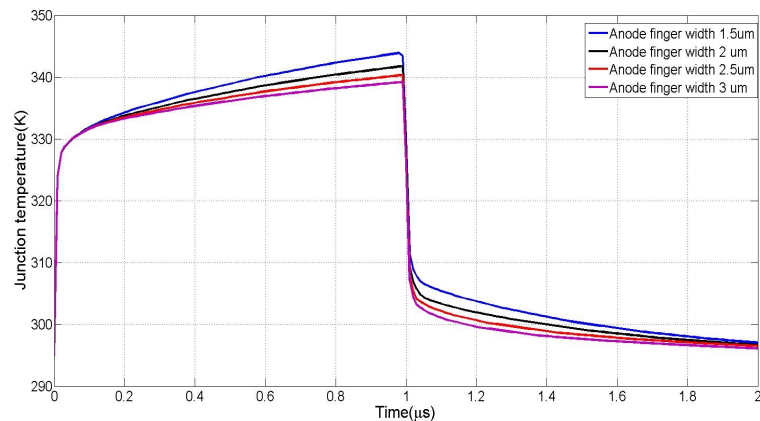


Figure 4.22: Test diode A temperature vs time with the variation of anode finger width with voltage 1 V, current 10 mA, and 1 μ s pulse length.

The width of the anode was also been varied. The material of the anode finger was gold. As the anode finger width increases, the amount of highly conductive materials increases. So heat flows away and junction temperature becomes less. A voltage pulse of $1 \mu\text{s}$ with a fall and rise time of 10 ns was applied again and the voltage amplitude was set to 1 V . Test diode A was simulated anode finger width varying from $1.5 \mu\text{m}$ - $3 \mu\text{m}$ with $0.5 \mu\text{m}$ step. The diode current for all variations was kept constant at 10 mA when the voltage is 1 V by changing the conductivity of the epilayer. A clear picture can be interpreted from Figure 4.22. At $1.5 \mu\text{m}$ the junction temperature was found to be around 345 K and at $3 \mu\text{m}$ the anode temperature around 338 K . A 7 K difference in temperature has been delineated with the variation of $2 \mu\text{m}$ width of the anode finger.

4.5 Temperature rise as a function of time

Theoretically the diode needs to be heated up for an infinite amount of time to reach steady state thermal equilibrium [24]. The epilayer and buffer layer material's heat capacity or specific heat of the diode is the main reason behind this phenomenon.

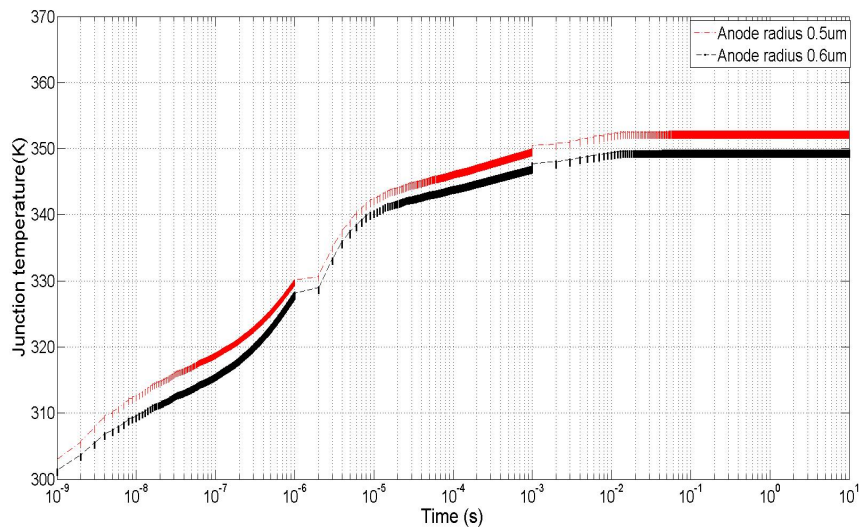


Figure 4.23: Temperature as a function of time for test diode B.

The transient thermal characteristics of test diode B can be found in Figure 4.23. The diode was exhibiting the transient behavior in microseconds and milliseconds range. Here two variation of test diode B with $0.5 \mu\text{m}$ anode radius and $0.6 \mu\text{m}$ anode radius have been simulated. The diode was demonstrating steady state behavior after 10 ms . The diode was heated up with 10 mW of power.

One problem with the COMSOL Multiphysics license was that only one million simulation steps were permitted. That is why these simulations have been done in 3 parts. The first step was 1 ns to $1 \mu\text{s}$ with a 1 ns step size, the second part $1 \mu\text{s}$ to 1 ms with a step size of $1 \mu\text{s}$ and the

third part 1 ms to 10 s with a step size of 1 ms. The combined simulation run time was about 3.5 hours. After every time step considered here the initial value and the outside temperature has been kept at 295.15 K.

Table 4.6: Simulation time (time dependent simulations) of Test diode C with different number of degrees of freedom and varying step size

Number of degrees of freedom to be solved	Simulation time (s)	Step size (s)	Number of steps
1342277	3912	10^{-6}	1000
1342277	4290	10^{-9}	1000
465071	4164	10^{-9}	1000
465071	3903	10^{-3}	1000

The simulation time for different number of degrees of freedom can be found in Table 4.6. The diode was not heated up for 10 s time continuously. The initial temperature was set to be 295.15 K. To tackle this problem two solutions have been considered. The first consideration is to change the ambient temperature of the second step to the final value of the first step. Here main consideration is given to the anode junction temperature so at the time the the second simulation starts the junction temperature would be the latest value and the diode will act as a continuously heated diode.

The second consideration is to change the initial value of the junction temperature of the second step to the final value of the first step. The ambient temperature of the diode is kept at constant 295.15 K.

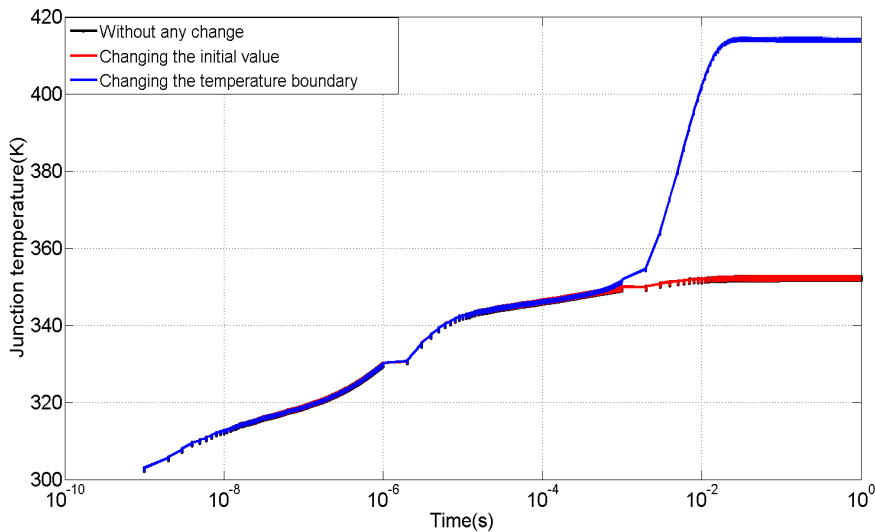


Figure 4.24: Test diode B temperature rise with time.

Test diode B was simulated using 10 mW of power and the diode was heated for a very long time. The three methods mentioned earlier have been compared. Test diode B exhibited the same result when the initial value of the junction temperature after the second step was changed to the final value of the first step and the whole time the initial value of the junction temperature was kept at ambient temperature 295.15 K. When the ambient temperature was changed the diode's behavior towards the rise of temperature changed towards the end completely and the temperature difference from the other two methods was found very significant. While using the first two methods the diode started to present steady state thermal behavior when the temperature was 352 K. But when the ambient temperature was changed the same behavior was found around 412 K, which differs from the other methods by almost 60 K. The third method were the ambient temperature was changed was not found reliable when test diode C simulated results were compared with measurement results.

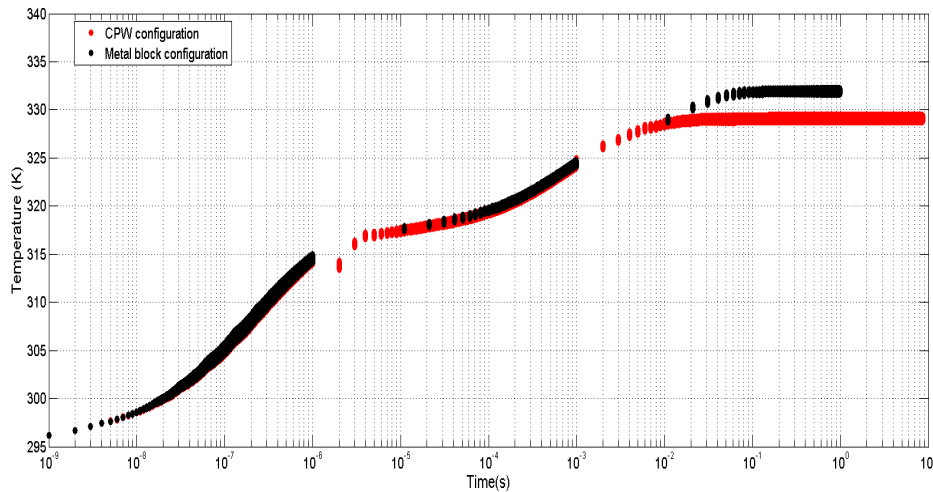


Figure 4.25: Test diode C temperature rise with time.

Next test diode C was heated up for a long time to see the temperature response using both of the CPW and metal block configurations. Both of the configurations were heated up with 10 mW of power for a very long time. The CPW configuration showed lower response than the metal block configuration in the milliseconds to onward region and reached thermal equilibrium faster than the metal block configuration. The highest temperature was found to be in the CPW configuration 328 K and metal block configuration 332 K. The diode was exhibiting transient behavior in microseconds and milliseconds range.

4.6 Thermal time constant extraction

To find out the thermal time constant the diode should be heated up for a long time and then the diode should let to cool down. The thermal response of the diode from the peak junction temperature to the local ambient temperature is fitted with exponential curves in MATLAB to

find out the thermal time constants. But the COMSOL license that is with us cannot simulate more than 1 million step points. That is why the the thermal time constants are extracted from the heating curves of the diode. Test diode C was used with 6.74 mW of power and the diode was heated for 10 seconds. The heating curve was then fitted with MATLAB curve fitting and 4 time constants were used to fit the curve with the simulated data. The diode was fitted with equation (4.1).

$$T = (T_1 \times (1 - \exp(\frac{-t}{\tau_1})) + (T_2 \times (1 - \exp(\frac{-t}{\tau_2})) + (T_3 \times (1 - \exp(\frac{-t}{\tau_3})) + (T_4 \times (1 - \exp(\frac{-t}{\tau_4})) + T_0, \quad (4.1)$$

Where T_1, T_2, T_3 and T_4 are the temperature coefficients and τ_1, τ_2, τ_3 and τ_4 are the thermal time constants T_0 is the ambient temperature.

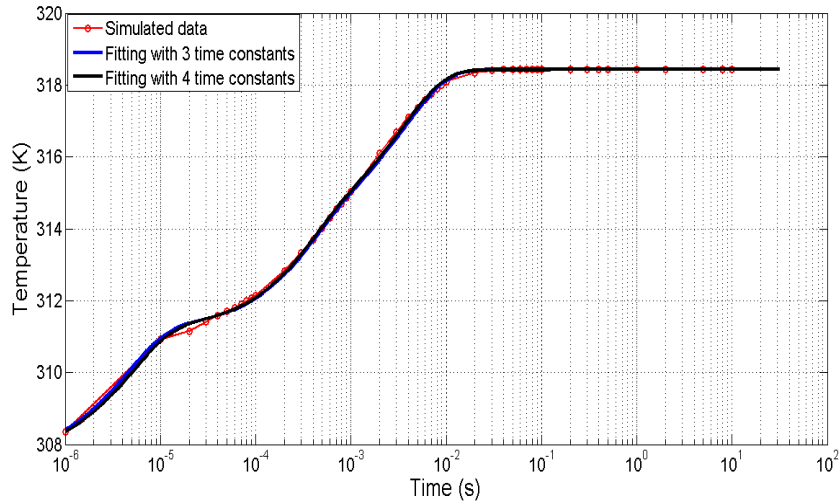


Figure 4.26: Test diode C thermal time constant extraction with MATLAB curve fitting for simulated results.

The thermal time constants and temperature coefficients can be found using equation (4.1) in the Table 4.7.

Table 4.7: Extracted thermal time constants

No. of time constants	T_1	T_2	T_3	T_4	τ_1	τ_2	τ_3	τ_4
4	3.538	2.998	8.191	3.986	$4.82^* \cdot 10^{-6}$	$3.48^* \cdot 10^{-4}$	0.0037	0.0036
3	3.512	2.993	4.217		$4.41^* \cdot 10^{-6}$	$3.59^* \cdot 10^{-4}$	0.0037	

4.7 Different heating time

This simulation was carried out to show how temperature of diodes rise when they are heated for different time. The two variations of the test diode B were taken in this case and they are heated with an ideal voltage pulses, that means the pulses have no fall or rise time, for a variable amount of time in the microseconds range. The pulse width was taken as 1, 2, 5, 10, 20, 50 μs . Temperature for different pulse length is different because of the Joule's law which can be found from equation (3.2).

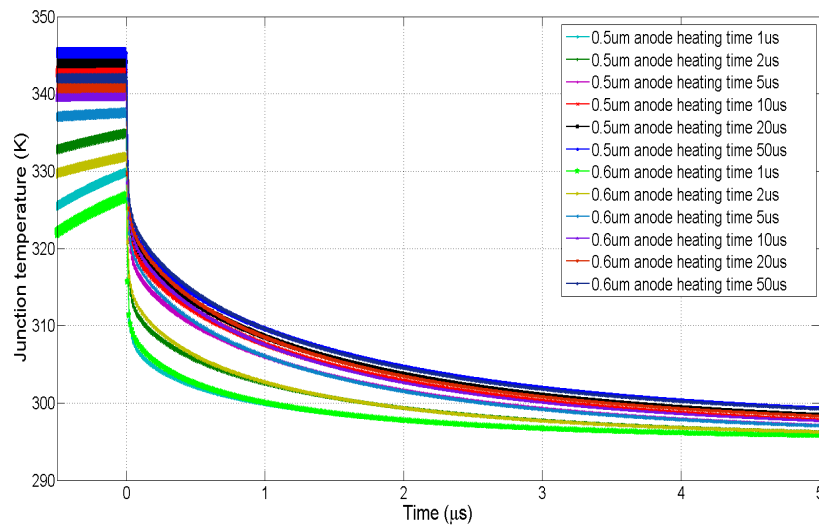


Figure 4.27: Test diode B junction temperature fall for different heating time.

Temperature will rise more if the diode is heated for a longer period. Also in the previous simulations the diode B with a 0.6 μm anode exhibited less junction temperature than the 0.5 μm anode radius diode B. This can be at a glance seen in Figure 4.27. The highest junction temperature was found when the diode B with radius 0.5 μm was heated up with a pulse width of 50 μs , which was about 345 K. The lowest junction temperature was exhibited by the 0.6 μm anode radius test diode B heated up with 1 μs .

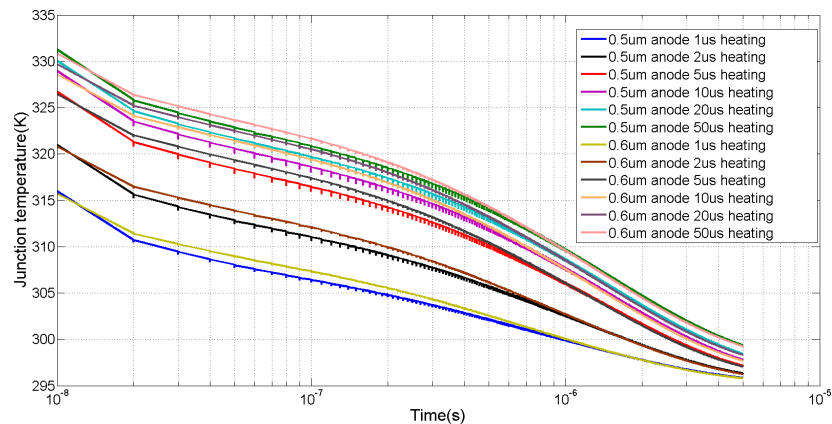


Figure 4.28: Test diode B temperature fall time in log scale.

Figure 4.28 presents the temperature fall of the diodes vs time in logarithmic scale. Though less temperature was found in the junction of test diode B with a variation of $0.6 \mu\text{m}$ anode when heated up with a longer pulsed voltage, more time is needed for the diode to cool down.

The junction temperature variation with the variation of different heating time can be more clearly depicted from Figure 4.28. Test diode B with the variation of $0.6 \mu\text{m}$ presents less junction temperature than the $0.5 \mu\text{m}$ anode test diode B. Here it also shows the temperature variation in the junction is more rapid when the pulse width is small than with bigger pulse widths.

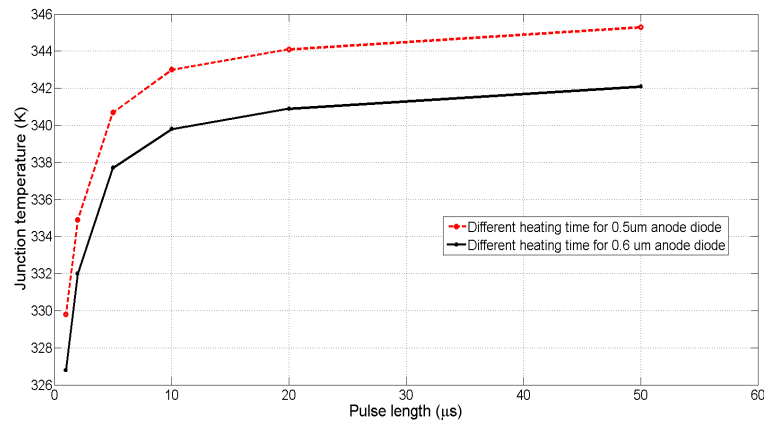


Figure 4.29: Test diode B peak junction temperature after different heating time.

Test diode C was heated up for different amount of time. While measuring this diodes it was not possible to get the peak temperature of the junction. Rather the diode was heated up for a long time and then the diode was let to cool down. While the diode was let to cool down the junction temperature was measured after some time was passed as there would be some instrumental effects present if the diode temperature is measured right after the diode is stopped being heated. However this problem does not persists in the simulations. So the diode is heated up for different amount of time and the diode was let to cool down for $15 \mu\text{s}$.

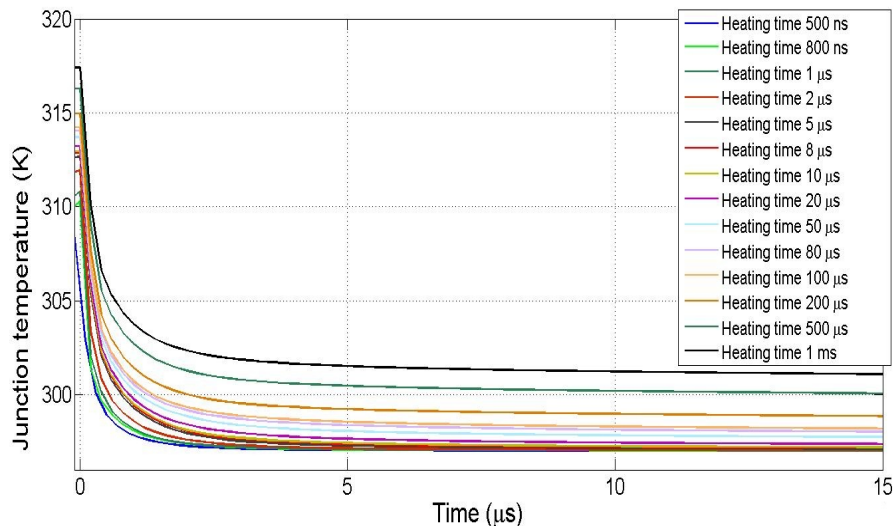


Figure 4.30: Test diode C cooling curves for different heating time.

Figure 4.30 shows the cooling curves after the diode is heated for different amount of time. Simulations have been carried out for 6.74 mW of power and for 500 ns, 800 ns, 1 μ s, 2 μ s, 5 μ s, 8 μ s, 10 μ s, 20 μ s, 50 μ s, 80 μ s, 100 μ s, 200 μ s, 500 μ s and 1 ms. From these cooling curves the junction temperature of the diode can be found out for a specific time period. In that way the junction temperature of the diode after the diode is cooled down can be found out. Also, with the COMSOL license does not permit to use more than 1 million data points. So using this process the characteristics of the diode while cooling down can be found.

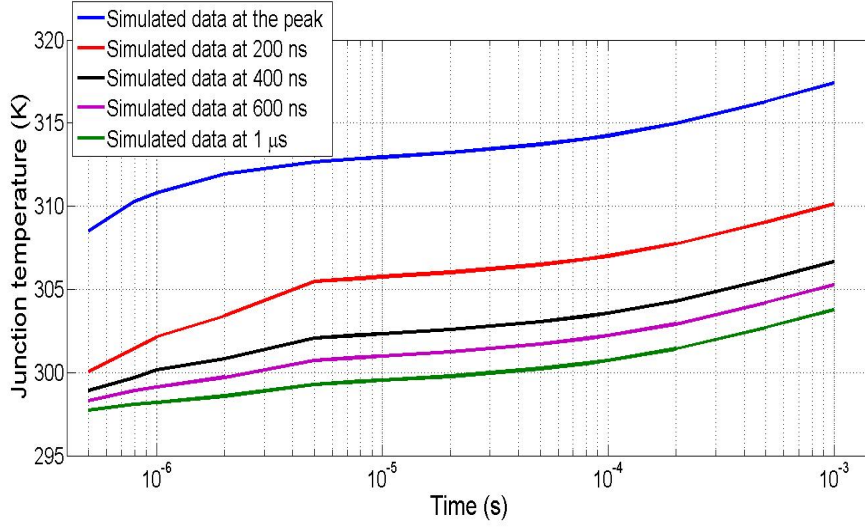


Figure 4.31: Test diode C temperature response from cooling curves.

From the cooling curves of test diode C the temperature response of the diode can be found. This temperature responses can be found in Figure 4.31. Data has been taken at the peak temperature and for 200 ns, 400 ns, 600 ns and 1 μ s. The simulations were carried out with the ambient temperature at 297 K and the CPW configuration of test diode C. In these simulations scenario the power that was supplied to the diode was kept constant.

4.8 Comparison with the measured results

In measurement and simulations, one diode test diode C, a varactor diode from Chalmers University of Technology, was common. In this section measurement results are compared with the simulated results. The measurement results are taken from [35]. For this work the ambient temperature was kept at 297 K and the diode was heated up for 10 s. There should be some variation as the power in the simulation is kept constant throughout the simulation. But in a practical case, the diode current rises with the temperature rise of the junction and the power is not constant. The power used in the simulation was kept constant at 6.74 mW. The peak junction temperature, thermal resistances and thermal time constants were compared with the measurement results.

The measurement process is carried out using a heating plate, a temperature sensor and

parameter analyzer. The diode was placed in the hot plate and the hot plate was heated up at known temperatures. The diode current changed with the heating according to equations (2.5), (2.6) and (2.4) and from this changed diode current and known heating plate temperature the temperature versus time curves were found out after performing calibration. The measurement procedure is in detail discussed in [35].

However, it was not possible to get the measurement results when the diode junction temperature was at peak. The diode was heated up for 10 s and data was taken 450 ns after the heating was finished. At that time the diode has already cooled down a bit. That is why the measured temperature is in some time frame lower than the simulated results as shown in Figure 4.32. As expected the measurement results should present more junction temperature than the simulated results. This excess junction temperature can happen because of the soldering that is used to attach the diode with the quartz substrate. The soldering effect is not discussed in this thesis and will further studied more. Moreover, in the simulations the diode current was kept constant but in reality the diode current increases with the increase of junction temperature and this increase in current will result to more junction temperature.

First the peak temperature of simulated results and measurement results after 450 ns were compared. The power that was selected for the comparison between measured and simulated results was 6.74 mW.

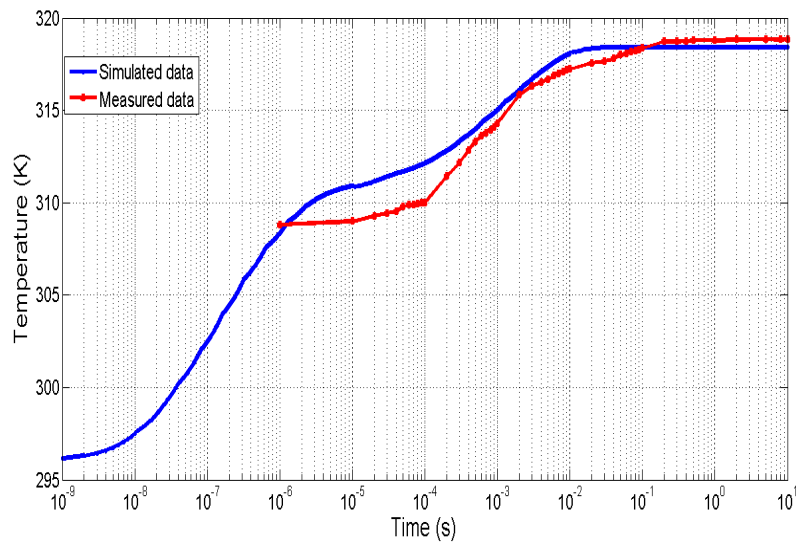


Figure 4.32: Comparison of measured and simulated results with 6.74 mW of power of test diode C temperature rise with time.

Figure 4.32 presents the difference between the measured and simulated results of the junction temperature as a function of time. The temperature difference was negligible and was as low as 0.4 K. The temperature difference might be more than 10-15 K between the simulated and measured results. The primary reason behind this is the soldering of the diodes. In this thesis the simulations done for test diode C had solder presented in the body of the diode. But for test diode C the solder was ideal. Although solder was used for test diode C in practical cases

the exact solder area and thickness cannot be determined and can be different for every diode. This excessive solder acts as a resistor and that resistor is responsible for the difference of heat between the measured and simulated results.

The thermal resistance was calculated for measured and simulated results for test diode C with the help of equation (2.13).

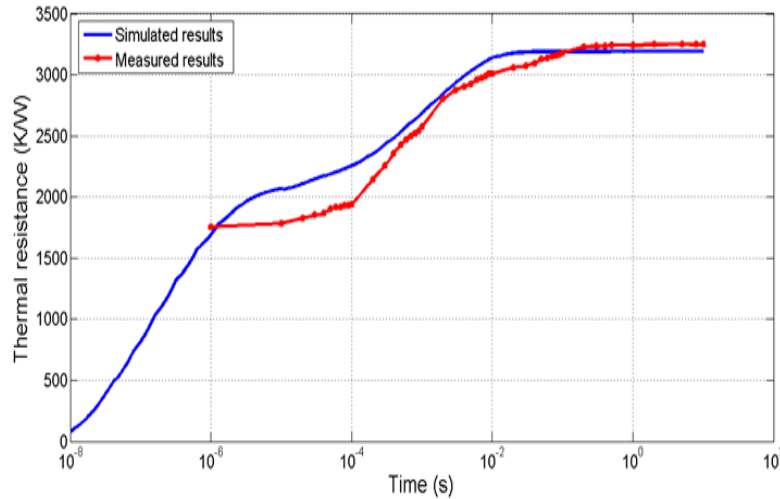


Figure 4.33: Comparison of measured and simulated results with 6.74 mW of power of test diode C thermal resistance.

The simulated maximum thermal resistance was found 3.191×10^3 and from measurement it was found at 3.252×10^3 . The difference of thermal resistance between the simulated and measurement results were found to be 60 K/W at the highest point.

To find out thermal time constants curve fitting was used and then the thermal time constants were found out using equation (4.1) and equation (2.21). Both the measurement and simulated temperature rise time with respect to time curves were fitted and thermal time constants extracted.

The measured temperature response with time curve was fitted in MATLAB and the thermal time constants were found out. As it is not possible to measure in lower than microseconds the curve was fitted with 3 time constants.

The measured heating curves have been fitted with three time constant with the help of MATLAB curve fitting. The extracted thermal time constant for the measured results can be found in Table 4.8.

Table 4.8: Extracted thermal time constants for measured results

T_1	T_2	T_3	τ_1	τ_2	τ_3
20.8	5.8	5.0	0.218×10^{-3}	1.7×10^{-3}	6.18×10^{-3}

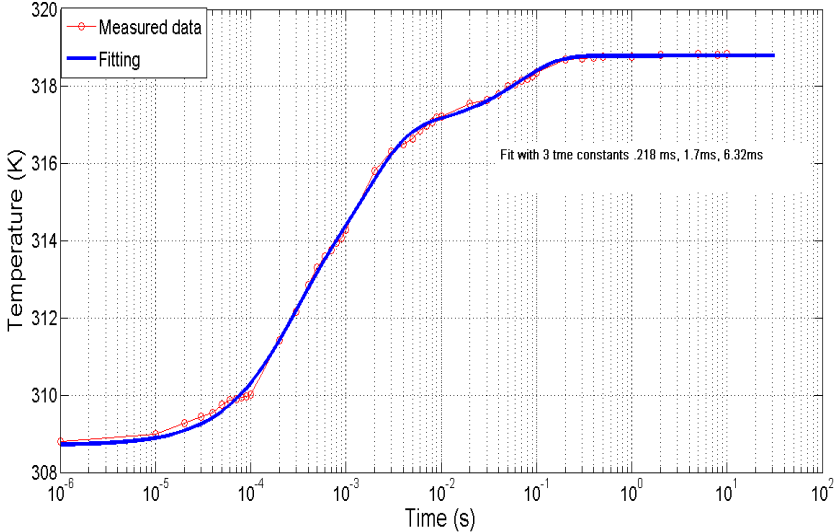


Figure 4.34: Test diode C thermal time constant with MATLAB curve fitting for measured results.

Chapter 5

Conclusion and future work

The reduced size of the anode junction for THz diodes degrades the thermal handling capabilities and the real electrical performance of the diode could not be determined. The thesis was aimed to build up an understanding of the thermal behavior of Schottky diodes. Especially the three thermal parameters junction temperature, thermal resistance and thermal time constant. All these three parameters are essential to characterize the Schottky diodes in terahertz range.

The 3 thermal characterization parameters namely junction temperature, thermal resistance and thermal time constant are studied in the thesis. At first a simple terahertz Schottky diode model with only the basic component of the diode was constructed. The analysis methodology was evaluated and then two commercial diodes, a varactor from Chalmers University of Technology and a mixer diode from ACST GmbH from Germany, were analyzed.

At first for test diode A, the difference between the simulated and calculated result was found around 8-9 K, which is 13 % of the total junction temperature. To find out where this heat is flowing away to a simple structure was simulated and it was confirmed the heat is flowing away from the buffer layer and the anode. Variation in the epilayer was an important concept as the epilayer was different from its real life counterpart. It was seen from the simulations that if the height of the epilayer was varied almost double the change of junction temperature was found around 1 K. When the radius of epilayer was varied the increase of 0.2 μm increased the junction temperature almost 1 K which is very low. Again temperature boundary, as it represents the heat finally flowing away was varied. The temperature boundary was set at the outer face of the anode finger and here the increase of 6 μm in the anode finger length increased the junction temperature by 6 K. The anode finger width was also varied and here with the increase of 1.5 μm width the junction temperature increased around 7 K.

The cooling curves of the diode could not be seen properly as the license that is present could not simulate more than 1 million data points. It took 1 hour with a CPU with 4 GB of RAM to simulate the Schottky diodes with 1000 step sizes. So to simulate these diodes with more than 10^7 step sizes would have taken a lot more time and almost impossible to simulate. However,

the heating of the diode was also simulated in 3 steps. First the diode was heated up to $1 \mu\text{s}$, then the diode was heated up to $1 \mu\text{s}$ to 1 ms range and at last the diode was heated upto 10 s range. This process was done in 3 ways. In one condition nothing was changed, in the second configuration only the initial value of the junction temperature was changed and at the last the temperature boundary was changed. The first two processes gave identical results and when compared with the measurement results the difference found was satisfactory. The 3rd and the last process exhibited 60 K more temperature than the other two processes and ruled out.

For the two commercial diodes the peak junction temperature was found around $325\text{-}345 \text{ K}$ for 10 mW of power. The Chalmers diode presented a maximum temperature of 328 K for CPW configuration and for the metal housing structure it showed the maximum temperature of 332 K . The difference in thermal resistance of the diode was found around 60 K/W at the peak temperature. The ACST diode exhibited a maximum junction temperature of 352 K . Both of the diodes went to thermal equilibrium around after 10 ms . Thermal time constants were found out for the Chalmers diode using the curve fitting tool in MATLAB. The curve fitting was done using 3 and 4 time constants.

Only one diode, the varactor diode from Chalmers University, was common for measurement and simulation. The temperature difference was found only 0.4 K between the measured and simulated results at the peak.

There are some future work that can also be done in the context of this thesis. Soldering plays a very important role in the thermal behavior of the Schottky diodes. Some soldering was used in the Chalmers varactor diode that is why the temperature difference between the measurement and simulated results were found this low. The effect of soldering in the diode's electrical and thermal characteristics can be further studied.

The simulations were done without the knowledge of the mobility of electron and holes, electrical conductivity of the epi and buffer layer and doping concentration of the buffer and epilayer. If these parameters are known, the diode can be simulated using the transport of diluted species in COMSOL and the results can be compared. This module can trace the flow of electron from the metal to the semiconductor.

Throughout the thesis the power supplied to the diode is kept constant. The current is not changing with the temperature as it supposed to be in a diode. To emulate a real life scenario of a diode the saturation current and the ideality factor should be modeled. The saturation current and ideality factors are all dependent on the junction temperature which is shown in equation (2.5) and equation (2.6) as [13]. The effect of junction temperature in ideality factor and saturation current is studied in [22] using some models. The effect of temperature in the ideality factor and saturation current can be further studied using the COMSOL simulation models used in this thesis.

Bibliography

- [1] S. M. Sze, *Semiconductor Devices, Physics and Technology*. John Wiley Sons, New York, USA, 1985.
- [2] C. Jansen, S. Wietzke, M. Scheller, N. Krumbholz, C. Järdens, K. Baaske, T. Hochrein, M. Koch, and R. Wilk, “Applications for THz systems,” *Optik & Photonik*, vol. 3, no. 4, pp. 26–30, 2008.
- [3] P. Siegel, “Terahertz technology,” *IEEE Transactions on Microwave Theory and Techniques*, vol. 50, no. 3, pp. 910–928, 2002.
- [4] M. Shur, “Terahertz technology: devices and applications,” in *Proceedings of the 31st European Solid-State Circuits Conference, 2005. ESSCIRC 2005*. IEEE, 2005, pp. 13–21.
- [5] T. Kiuru, *Characterization, Modeling, and Design for Applications of Waveguide Impedance Tuners and Schottky Diodes at Millimeter Wavelengths*. Ph.D dissertation, Aalto University School of Electrical Engineering, Department of Radio Science and Engineering, Finland, 2011.
- [6] A. Tang, *Modelling of Terahertz planar Schottky diodes*. Licentiate thesis, Chalmers University of Technology, Sweden, 2011.
- [7] S. M. Sze and K. K. Ng, *Physics of Semiconductor Devices*. John Wiley Sons Inc., Hoboken, NJ, USA, 2007.
- [8] P. J. Singh, “Semiconductor devices: Basic principles site,” chapter 7. [Online]. Available: <http://web.eecs.umich.edu/~singh/bk7ch07.pdf>
- [9] M. Faber, J. Chramiec, and M. Adamski, *Microwave and Millimeter-Wave Diode Frequency Multipliers*. Artech House, Norwood, MA, USA, 1995.
- [10] S. Montanari, *Fabrication and Characterization of Planar Gunn Diodes for Monolithic Microwave Integrated Circuits*. Ph.D. dissertation, RWTH Aachen, Aachen, Germany, 2011.

- [11] E. H. Rhoderick, "The physics of Schottky barriers?," *Review of Physics in Technology*, vol. 1, no. 2, p. 81, 1970.
- [12] F. Padovani and R. Stratton, "Field and thermionic-field emission in Schottky barriers," *Solid-State Electronics*, vol. 9, no. 7, pp. 695–707, 1966.
- [13] C. Crowell and V. Rideout, "Normalized thermionic-field (t-f) emission in metal-semiconductor (Schottky) barriers," *Solid-State Electronics*, vol. 12, no. 2, pp. 89–105, 1969.
- [14] T. W. Crowe, R. J. Mattauch, R. M. Weikle, and U. V. Bhapkar, "Terahertz GaAs devices and circuits for heterodyne receiver applications," in *International Journal of High Speed Electronics and Systems*, vol. 6, no. 1, pp. 125–161, 1995.
- [15] A. Bar-Cohen and A. Kraus, *Thermal Analysis and Control of Electronic Equipment*. McGraw Hill/Hemisphere Publishing Coproration, New York, USA, 1995, vol. 2.
- [16] P. Baureis, "Electrothermal modeling of multi-emitter heterojunction-bipolar-transistors (HBTs)," in *Third International Workshop on Integrated Nonlinear Microwave and Millimeterwave Circuits, Duisburg, Germany*, Oct. 1994, pp. 145–148.
- [17] D. J. Walkey, T. J. Smy, T. Macelwee, and M. Maliepaard, "Compact representation of temperature and power dependence of thermal resistance in Si, InP and GaAs substrate devices using linear models," *Solid-State Electronics*, vol. 46, no. 6, pp. 819–826, 2002.
- [18] D. Dawson, "Thermal modeling, measurements and design considerations of gaas microwave devices," in *16th Annual Gallium Arsenide Integrated Circuit (GaAs IC) Symposium, Philadelphia, Pennsylvania, USA*, Oct. 1994, pp. 285–290.
- [19] J. Stake, L. Dillner, S. Jones, C. Mann, J. Thornton, J. Jones, W. Bishop, and E. Kollberg, "Effects of self-heating on planar heterostructure barrier varactor diodes," *IEEE Transactions on Electron Devices*, vol. 45, no. 11, pp. 2298–2303, Nov. 1998.
- [20] M. Ingvarson, B. Alderman, A. Olsen, J. Vukusic, and J. Stake, "Thermal constraints for heterostructure barrier varactors," *IEEE Electron Device Letters*, vol. 25, no. 11, pp. 713–715, Nov. 2004.
- [21] A. Tang, E. Schlecht, G. Chattopadhyay, R. Lin, C. Lee, J. Gill, I. Mehdi, and J. Stake, "Steady-state and transient thermal analysis of high-power planar Schottky diodes," in *22nd International Symposium on Space Terahertz Technology, Tucson, AZ, USA*, April, 26-28 2011.
- [22] T. Kiuru, J. Mallat, A. Räisänen, and T. Närhi, "Schottky diode series resistance and thermal resistance extraction from s-parameter and temperature controlled I-V measurements," *IEEE Transactions on Microwave Theory and Techniques*, vol. 59, no. 8, pp. 2108–2116, Aug. 2011.

- [23] H. Zirath, "High-frequency noise and current-voltage characteristics of mm-wave platinum $n-n^+$ -GaAs Schottky barrier diodes," *Journal of Applied Physics*, vol. 60, no. 4, pp. 1399–1407, 1986.
- [24] J. Sofia, "Fundamentals of thermal resistance measurement," 1995, 2012.05.21. [Online]. Available: <http://ssl.xmu.edu.cn/download%5CThermal%5CFundamentals%20of%20Thermal%20Resistance%20Measurement.pdf>
- [25] B. Boley and J. Weiner, *Theory of Thermal Stresses*. John Wiley and Sons, Inc., New York, 1960, pp. 138-141.
- [26] M. Thirumaleshwar, *Fundamentals of Heat and Mass Transfer*. Dorling Kindersely India Pvt. Ltd, 2006, pp. 13-18.
- [27] S. Adachi, *Properties of group-IV, III-V and II-VI semiconductors*. John Wiley Sons Inc., Chichester, West Sussex, England, 2005, pp.33-38.
- [28] D. Blackburn, "Temperature measurements of semiconductor devices - a review," in *Twentieth Annual IEEE Semiconductor Thermal Measurement and Management Symposium, San Jose, CA, USA*, Mar 2004, pp. 70 – 80.
- [29] G. Gray, *Molecular Structure and Properties of Liquid Crystals*. Academic Press Inc. London Ltd., 1962.
- [30] K. Azar, J. Benson, and V. Manno, "Liquid crystal imaging for temperature measurement of electronic devices," in *Seventh Annual IEEE Semiconductor Proceedings Thermal Measurement and Management Symposium, 1991. SEMI-THERM VII. Phoenix, AZ, USA*, Feb 1991, pp. 23–33.
- [31] I. Baylis, C.P. and L. Dunleavy, "Understanding pulsed IV measurement waveforms," in *The 11th IEEE International Symposium on Electron Devices for Microwave and Optoelectronic Applications*, Nov. 2003, pp. 223–228.
- [32] L. Dunleavy, W. Clausen, and T. Weller, "Pulsed IV for nonlinear modeling," *Microwave Journal*, vol. 46, no. 3, pp. 68–85, 2003.
- [33] A. Technologies, "High frequency transistor primer, part iii thermal properties," May 12th 2012. [Online]. Available: http://paginas.fe.up.pt/~hmiranda/etele/trans_primer3.pdf
- [34] "It's a multiphysics world," June 7th 2012. [Online]. Available: <http://www.comsol.fi/multiphysics/>
- [35] S. Khanal, *Pulsed and Transient characterization of THz Schottky diodes*. Master's thesis, Aalto University School of Electrical Engineering , Department of Radio Science and Engineering, Finland, 2011.